Front-end and Back-end of a 100-200 MHz radio telescope focused on the cosmological study of the Epoch of Reionization

MSc Felipe P. Mosquera

Degree work to qualify for the title of Master in Telecommunications

Director

Julián Rodríguez Ferreira

PhD Physics

Co-directors

Efrén Darío Acevedo Cárdenas

MSc Electronic Engineering

Oscar Alberto Restrepo Gaitan

MSc Astronomy

Universidad Industrial de Santander

Facultad de Ingenierías Fisicomecánicas

Escuela de Ingenierías Eléctrica, Electrónica y de Telecomunicaciones

Bucaramanga

2022

Dedication

This thesis is dedicated to Mona and Tati.

Acknowledgements

Thanks to my family and close friends. Also to my director and co-directors for all their support.

Contents

List of Figures

List of Tables

List of appendix

pág.

Abstract

Title: Front-end and Back-end of a 100-200 MHz radio telescope focused on the cosmological study of the Epoch of Reionization.

Author: MSc Felipe P. Mosquera Facultad de Ingenierías Fisicomecánicas Escuela de Ingenierías Eléctrica, Electrónica y de Telecomunicaciones.

Director: Julián Rodríguez Ferreira Ph.D Physics.

Keywords: Radiotelescope, SDR, radioastronomy.

Description: Radio astronomy as a science allows among others experimental validation of theoretical models based on the study of electromagnetic cosmic waves. Technically, it uses dedicated instrumentation (radio telescopes) to acquire such signals. This study, based on the emission of 21-cm of neutral hydrogen at frequencies between 100 and 200 MHz, allows us to examine a scientific case of open study from signals emitted during the Epoch of Reionization (EoR) of the universe in which we seek to compare physics models with experimental measurements.The EoR study allows us to understand the dynamic systems present at a primordial universe epoch based on the behavior of electromagnetic waves. This project is based on simulations and measurements of a radioreception system which integrates an antenna, transmission lines, a pre-amplifier and a receiver, and also the development of a software solution for data pre-processing, compatible with Software Defined Radio (SDR) receivers. The aim is to validate the response of the antenna and the subsystems to establish the feasibility to use SDR technology devices as receivers for low-frequency radio telescopes. This project contributes to radio astronomy initiatives underway at the Universidad Industrial de Santander (UIS), which seek to position the university as a national and regional reference in this area of study.

Introduction

The study of the 21-cm line of neutral hydrogen emitted during the Epoch of Reionization (EoR) of the universe is an open scientific case. This allows the study of the mechanisms of formation of the first stars and galaxies generated in the early universe (Barkana and Loeb, 2005), and the ionization processes of the original gas (Furlanetto et al., 2006). In 2018, a detection of this signal reported by The Experiment to Detect the Global Epoch of Reionization Signature (EDGES) (Bowman et al., 2018) opened an academic and scientific debate on the non-correspondence of the current physical models vis-à-vis the reported signal (different amplitude levels with respect to temperature) (Pritchard and Loeb, 2012) (Monsalve et al., 2017b). Worldwide, there are different initiatives for the study of the proposed case. These initiatives use two types of antenna configurations: single antennas or interferometric arrangements. We present the design and implementation of a complementary prototype of a low-frequency radiotelescope. Our prototype considers an independent antenna designed to operate in the frequency range between 100 and 200 MHz. The antenna is based on the one used in the High-Frequency instrument of the EDGES project (Monsalve et al. (2017a) and includes a novel receiver based on Software Defined Radio (SDR) technology. This project will verify the pertinence of using this technology for low-frequency radio astronomy.

This project is supported by ongoing related initiatives that seek to consolidate the UIS as a national reference in the study of radio astronomy. This system will merge with a radio astronomy station of UIS framed in the project *"Desarrollo de un arreglo interferométrico de Radio Telescopios para establecer una estación de Radio Astronomía de la UIS en el Páramo de Berlín (San-*

tander)". Also, it will be used for the project *"Caracterización de emisiones electromagnéticas de interferencia de radiofrecuencias y pruebas de un radio telescopio (100mhz) como insumos para la validación del sitio de montaje de una base radio astronómica en la península antártica* (*fase cero dentro del Programa Radio Astronómico Antártico Colombiano (PRAC)"*. Both initiatives will contribute to the country's scientific and technological development.

Likewise, this initiative permits future projects in data calibration, design and implementation of dedicated radio astronomy instrumentation, and data post-processing oriented to the cosmological study of this scientific case.

The following document is divided into 7 sections: background, radiotelescope system description, simulations, measurements, results, future work and conclusions. Initially, the theoretical framework is presented, where basic concepts of radio astronomy such as the atmospheric window of radio frequencies and characteristics of radio telescopes are mentioned. Subsequently, the scientific case study, instruments used, and related systems are described. Chapter 2 describes the radio telescope covering the front-end components (antenna and receiver) and the back-end software architecture developed. Chapter 3 presents the antenna S_{11} parameter and chromaticity simulations. Chapter 4 presents the antenna S_{11} parameter measurements, sensitivity and linearity for three SDR radios, and the S_{21} parameter of the pre-amplifier. Chapter 5 presents the results obtained from effective area and source temperature calculations to determine the total system temperature. This temperature is evaluated considering the system without pre-amplifier, with the current pre-amplifier and a recommended pre-amplifier. Additionally, a comparison of the measurements vs. simulations of the antenna, a comparison of the SDR measurements and the results

of the total integrated system, and the first in-situ data collection are presented. Finally, the activities to be carried out for the continuity of this project are presented in Chapter 6 and the conclusions in Chapter 7.

Objectives

0.1. General Objective

- Validate a 100-200 MHz radio telescope oriented to the cosmological study of the reionization epoch using SDR-technology.

0.2. Specific objectives

- Produce a model to establish the performance of the radio telescope by the generation of simulations and measurements of each subsystem.
- Define a software architecture compatible with the SDR receptor capable of processing and visualizing the data from the incoming signals.
- Perform the integration of the subsystems to establish a fully operable low-frequency radio telescope.
- Analyze the data collected from in-situ measurements to evaluate and define the system's validity.

1. Background

This project is oriented to validate low-frequency radio telescope subsystems in order to integrate a radio receiver system designed for an astrophysical research problem. First, the fundamentals of radio astronomy are explained. Then the study case Epoch of Reionization (EoR), and similar projects and instruments were carried out.

1.1. Radio Astronomy

The serendipitous findings of Karl Jansky in 1933 became the birth of radio astronomy. He was an electrical engineer assigned to locate the source of interferences of the transatlantic radiotelephone of Bell Laboratories. His findings turned out to be the first measurements of cosmic radio waves, which were emitted from the Milky Way.

Radio astronomy is a science used to study cosmic radio waves. These waves originate from different radio sources such as stars, nebulae, galaxies, pulsars, the Sun, planets (by black body temperature emission), the intergalactic medium, molecule emission lines and the Cosmic Microwave Background (CMB). By studying these waves is possible to understand the origin (place and emission mechanism) and the type of object under study. Likewise, the chemical composition, evolution and distances of the emission sources (due to red-shift behavior) (Burke and Graham-Smith, 2009b). In radio astronomy, the Jansky unit (Jy) is used as a standard unit for measuring the intensity of a signal, which represents the radio-energetic measurement by area at a specific frequency. One Jansky is equivalent to 10^{-26} W/m$^2 Hz$.

1.1.1. Atmospheric window (radio frequency transparency). Electromagnetic waves are framed within the electromagnetic spectrum, classifying waves based on their frequency. As shown in Figure 1, the highest frequencies correspond to Gamma Rays and the lowest to Radio.

Figure 1
Electromagnetic spectrum segmented by bands.

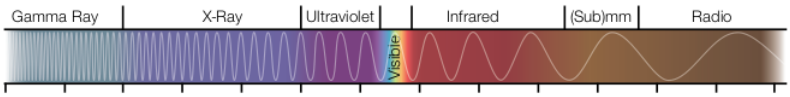

Note. Adapted from Burke and Graham-Smith (2009b)

The atmospheric window concept infers how the atmosphere blocks or absorbs certain radiations. Therefore, not all cosmic waves are perceptible from Earth. As seen in Figure 2, the atmosphere absorbs the most significant portion of electromagnetic radiation, a concept known as opacity. The Radio band, visible and some near ultraviolet and infrared regions are transparent for the atmosphere. These are the regions where ground-based optical telescopes and radio telescopes are functional. The other ranges are studied using telescopes placed in orbit where the atmospheric window does not affect the obtainment of these waves.

1.1.2. Radio telescopes. Optical telescopes are usually conceived as the only tool for the experimental study of the universe. They use the visible range of the electromagnetic spectrum, while radio telescopes are designed to acquire electromagnetic signals in the radio wave range. For almost 70 years, radio telescopes have made possible the confirmation of theories related to the conformation and processes of our cosmos and contributed to the upcoming of new technologies and instrumental techniques (Wilson et al., 2012). Radio telescopes are designed to

Figure 2
Atmospheric window; cosmic waves filtration.

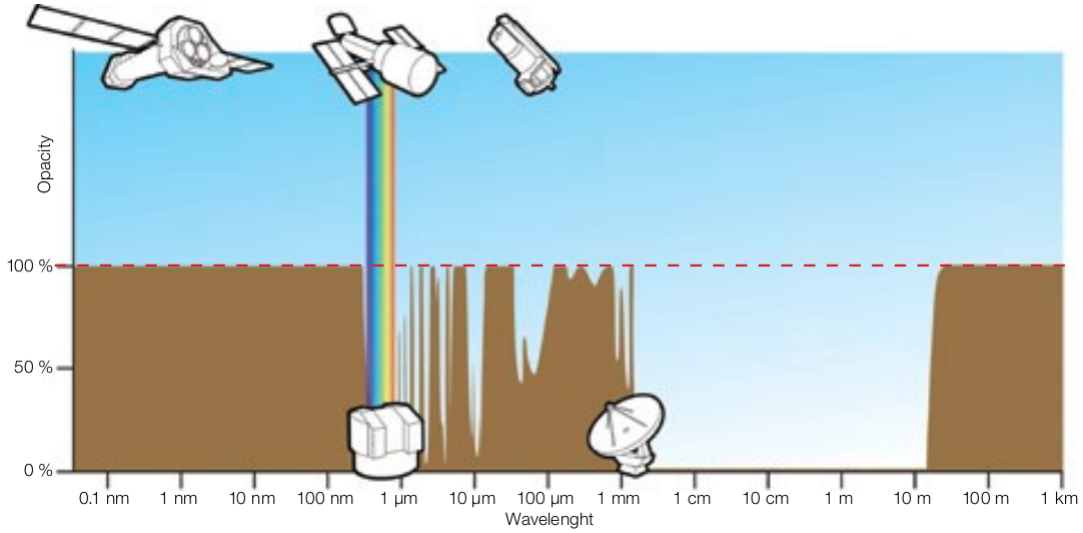

Note. Adapted from (Burke and Graham-Smith, 2009b)

capture electromagnetic waves of cosmic origin. Technically, they integrate the necessary subsystems to capture and pre-process cosmic signals. There are different configurations according to the study case or research area. These cases define the requirements regarding the construction of antennas, receiver systems, amplifiers, filters, signal switching, cleaning methods for parasitic signals, information storage, and data collection protocols, among others (Burke and Graham-Smith, 2009a).

Although radio telescopes can inherit radio-telecommunications technologies, the instrumentation for astronomy observations differs mainly in the high levels of sensitivity required to obtain and process the very faint incoming cosmic signals. Traditionally, a dedicated receiver is designed and implemented for every specific application. These receivers and front-ends have several stages of filtering and amplification and sometimes are cooled by cryogenic systems to

increase the sensitivity to process the faint signals. They are also built to work for the specific bandwidths required for each scientific case. In terms of the antennas, high-performance radio telescopes use tailor-made feeders and a high accuracy surface's roughness for parabolic reflectors. This roughness is a crucial parameter when sub-millimeter signals are studied. In our case, the instrumentation used to study low frequencies contemplates different antenna geometries such as monopoles, cone log spiral, and for our case, blade dipole. Such geometries provide cost and size reduction and structural benefits in terms of weathering requirements. On the other hand, since the case study does not require a significant directivity, the beam shape of the antennas mentioned above allows obtaining beam widths equal to or greater than 60 degrees.

1.2. Study of 21-cm signals

1.2.1. 21-cm line. The scattering of ultraviolet radiation from ancient stars altered the state of excitation of hydrogen atoms (hyperfine line in 21-cm) (Ali, 2004); the wavelength of the neutral hydrogen @ 1.4GHz is 21 centimeters. This alteration caused the hydrogen gas to absorb photons from the cosmic microwave background, generating spectral distortion currently observable at ranges between 40 and 200 MHz. It is found as faint isotropic radiation. For terrestrial detection, it matches multiple telecommunications bands, demanding RFI silent locations. The measurements corresponds to a differential brightens temperature dependable on the neutral hydrogen fraction and the spin temperature of the gas (Monsalve et al., 2017b).

1.2.2. Redshift. Redshift is a relation, expressed as z, that contemplates the increase of a wavelength, contrasting the difference between the observed and the original emitted wavelength of an electromagnetic wave by the Doppler effect.

1.2.3. Cosmic Dawn (CD) and Epoch of Reionization (EoR). The universe was hot and dense after the Big Bang took place (ionized gas medium). Around 380.000 yr later, it started cooling, and the first Hydrogen atoms formed. This era is known as the Dark Ages (DA). Then after 400 ml yr. The formation of the first stars due to gravitational forces began. This period is called Cosmic Dawn (CD). The interaction of waves from these stars with the neutral Hydrogen environment produced ionization processes; this is the Epoch of Reionization of the universe. The 21cm signal of the cosmic awakening Cosmic Dawn (CD) and EoR with redshifts (z) between 6-30 (Figure 3) helps to understand the nature of the primordial radiation sources and the physics of the intergalactic medium.

Figure 3
21-cm signal model.

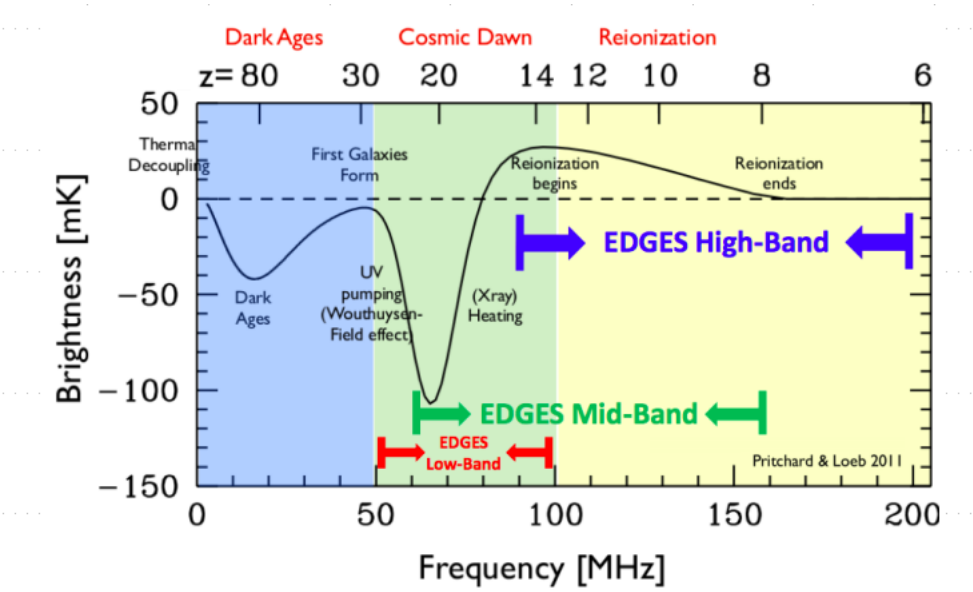

Note. Frequency vs Brightness graph of the 21-cm signal in the early ages of the universe. Adapted from Monsalve et al. (2017b).

Due to cosmological reionization, most of the gas in the universe is ionized around a z=6.

This scientific case allows studying the nature and properties of the first sources of radiation that transformed the thermal and ionization states of baryons in the universe and to specify timelines of the heating and reionization phases (sequence of events during CD and EoR) (Mozdzen et al., 2016).

1.2.4. Ionospheric effects. Regions of HII in the galaxy block background emissions at low frequencies. These regions are mainly observed on the galactic plane (monotonic spectrum). The radiofrequency recombination lines are close absorption lines (0.5MHz). The Earth's ionosphere absorbs radio signals at low frequencies and produces thermal radiation from hot (excited) electrons. Measurements must consider ionospheric conditions to make the corresponding corrections in the models used. "The absorption profile at 21-cm is the continuous superposition of gas lines through the redshift (z) and the cosmological volume; the shape of the profile traces the history of the gas in time (cosmic) and is not the result of a single gas cloud (v = 1,420 / (1 + z) MHz)" (extracted from (Bowman et al., 2018)). The intensity of the 21-cm signal from the early universe is represented by the brightness temperature relative to the microwave background radiation (Costa, 2018).

1.2.5. EDGES and reported spectrum. The Experiment to Detect the Global Epoch of Reionization Signatures (EDGES) was implemented in 2015 at the Murchinson radio observatory and designed to measure the absorption profile in 21-cm (Monsalve et al., 2018). It consists of 3 main instruments: EDGES Low band (frequency band 50-100 MHz for a redshift 30>z>14), EDGES Mid Band (frequency band 60-160 MHz for a redshift $25 > z > 8$), and EDGES High band (frequency band 90-200 MHz for a redshift $15 > z > 6$) (Figure 3). These

systems comprise dedicated tailor-made receivers and blade dipole antennas. The receiver has a switch stage that allows connection to calibration loads, measurement equipment (VNA), and directly to the antenna. It uses noise sources to perform the calibration to obtain temperature scale measurements. The antenna is a blade-type single-polarization zenith dipole on a ground plane. Impedance matching is managed through a Roberts balun integrated into the antenna. The expected spectral signature is between 50 and 200 MHz with an amplitude peak between 10 and 200 mK, depending on the star formation model (Mozdzen et al., 2016). The EDGES observations get an emission profile in which the magnitude of the signal amplitude is 2 to 4 times greater than the results from physical models. There are still not known astrophysical mechanisms that explain what was captured. Radiation from stars and stellar remnants itself does not explain it either. However, two dominant theories intend to explain this discrepancy. Either the original gas was colder than contemplated (as a result of the interaction of dark matter with baryons), or the temperature of the cosmic radiation was hotter (due to the decay of dark matter or evaporation of primordial black holes). Low-frequency profiles (50-100 MHz) show the existence of stars that produced Lyman-alpha photon background radiation 180 million years after the Big Bang. The high-frequency profiles (90-200 MHz) indicate that the gas was heated below the radiation temperature less than 100 million years later (Bowman et al., 2018).

1.3. 21-cm state of art projects

There are a growing number of radio reception systems or radio telescopes at low frequencies for the study of the 21-cm line (Parsons, 2011) (Mazumder and Datta, 2019). In terms of the antennas, they mainly vary in the use or not of a balun Yuan et al. (2018) and (Raghunathan

et al., 2013), beam chromaticity Price et al. (2018), and calibration methods (switching of passive loads). These methods are designed to evaluate system efficiency and independence in frequency of the beam pattern (chromaticity). Chromaticity in an antenna expresses the variation of gain with respect to frequency and elevation angle and is a crucial parameter for studying the 21-cm line. This antenna beam chromaticity may result in a delayed power spectrum affecting the results of the measurements (Thyagarajan et al., 2016). Also, the antennas do not require a high spatial resolution since it is a sky-global signal, although it is of great importance that the highest beam gain is at the zenith. The expected 21-cm cosmic signal is very faint i.e., maximum amplitude = 300 mK (brightness temperature) and frequencies between 40-200 MHz. This signal is immersed in noise or galactic foreground i.e., maximum amplitude = 100 - 10.000 K (brightness temperature) and frequencies between 10-320 MHz. These considerations demand high degrees of efficiency and high reliance on every component. For instance, the target parameters for the receptor are input return loss $>$10 dB, gain 10 - 30 dB, output return loss $>$10 dB, and noise figure between 0 and 4 dB, and for the receptor amplifiers a nominal impedance of 50 Ohms, frequency range 100-200MHz and temperature range between -20 and 40 degrees Celsius (Bowman et al., 2018).

1.3.1. Current projects. Nowadays, several systems based on single and interferometric antenna configurations cover this case study. Among the interferometric arrangements, there are: the Long Wavelength Array (LWA) (Ellingson et al., 2009), Murchinson Widefield Array (MWA) (Ord et al., 2019), Precision Array for Probing the Epoch of Reionisation (PAPER), Low-Frequency Array (LOFAR) (Offringa and de Bruyn, 2011), and Large Aperture experiment to detect Dark Ages (LEDA) (Price et al., 2018). Considering the systems with a single antenna,

there are: the Cosmological probe of the Islands for the detection of neutral (HSCI-HI) , Probing Radio Intensity at high z from Marion (PRIZM), Shaped Antenna measurement for the background Radio Spectrum (SARAS2) (Singh et al., 2018), Hydrogen Epoch of Reionization Array (HERA) DeBoer et al. (2017), Mapper of the IGM Spin Temperature (MIST), Broadband Instrument for Global Hydrogen ReioNisation Signal (BIGHORNS) (Sokolowski et al., 2015), The Radio Experiment for the Analysis of Cosmic Hydrogen (REACH), The Cosmic Twilight Polarimeter (CTP) and High-Z . Table 1 presents a comparison of some radio astronomical systems for the EoR study mentioning operating frequencies, type of antenna, the use of a balun, calibration scheme, and type of spectrometer.

Table 1

Comparison between low frequency systems for the study of the 21-cm emission.

System	Frequency range (MHz)	Antenna type	Use of balun	Calibration scheme
SARAS2	40-200	spheric monopole	no	coupled noise source
EDGES	100-200 50-100	blade	yes	antenna and noise source commutation
BIG HORNS	70-200	cone log-spiral	yes	antenna and reference source commutation
SCI-HI	40-130	hibiscus	yes	antenna, 50 and 100 Ohms loads and short terminal commutation
LEDA	40-85	double polarization dipole	yes	antenna and noise source commutation combined with cross-correlation of other antennas
MIST	40-125	blade dipole	yes	reference source calibration and soil calibration

2. Radiotelescope system description

The following is a description of the radio telescope subsystems. First, the implemented antenna and the characteristics of the balun are described. Subsequently, the use of SDR technology in radio astronomy applications and the Limenet mini architecture are mentioned. Finally, the software architecture development is explained.

The system is segmented into several sub-systems as shown in Figure 4.

Figure 4
Subsystems of the radiotelescope to be validated

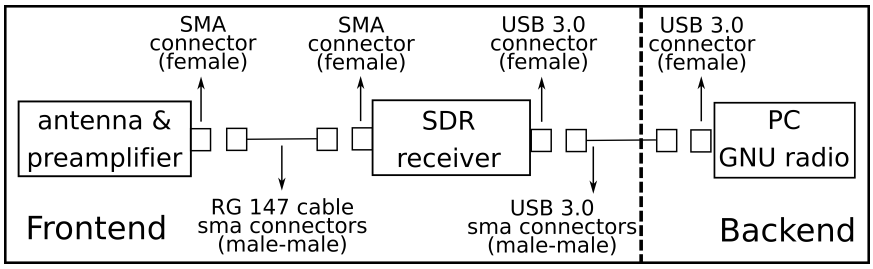

2.1. Blade antenna

The High Band EDGES antenna inspired the UIS antenna for the EoR study. Our antenna is a single polarization dipole-like blade composed of two rectangular aluminum sections (Monsalve et al., 2017a) (62.5 $\times$ 48.1 cm) raised 52 cm from a rigid aluminum plate (1.3 $\times$ 1 m) used as the ground plane (see Figure 5(bottom left)). This ground plane was complemented using four sections of wire grid panels; two panels with dimensions 5 $\times$ 2 m and two panels of 1.85 $\times$ 1 m. The overall dimension of the ground plane is 5 $\times$ 5 m. The structure of the antenna was built in polystyrene

[1] . A Roberts balun was implemented using two copper tubes attached by a movable aluminum plate (balun tuner) (see Figure 5 (bottom right)). This balun electrically balances the incoming signal. The balun tuner permits electrical length and transmission line impedance adjustment and calibrates the antenna response in terms of the bandwidth and central frequency. An aluminum case was used to shield vertical currents in the copper tubes Monsalve et al. (2017a). The port consists of a sma connector placed between the copper rod and one of the copper tubes. This antenna was designed to operate in frequencies between 100 and 200 MHz.

The Roberts Balun, also known as Collins Balun, converts a balanced output (from the antenna) to an unbalanced output. This type of balun is also used to extend the bandwidth of the antenna match. Figure 6 presents the correspondent transmission line circuit, where A represents a ¼ wave transformer (transmission line), B a shorted balanced line, C an open stub line (open-ended line), and D the tuner. Za, which is the antenna impedance, is in parallel with B. The unbalanced port is introduced through A and connected in series to the antenna by C. The lengths of A and B can be reduced by the D. The impedance of B is defined by ZB=$R_b(1+\Gamma)/(1-\Gamma)$, where $\Gamma = -e^{i\phi_b}$, R_b is the line impedance, $\phi_b = -4\pi l\varepsilon^{\frac{1}{2}} f/c$ (being l the length, f the center frequency, c the velocity of light and ε the dielectric coefficient) (Roger, 2012).

---

[1] Polystyrene was used to build the strucure for cost-effective solution in terms of low thermal conductivity among the possible materials available (diffusivity = 0.026x10-6 m2/s)

Figure 5
UIS 100-200 MHz blade antenna.

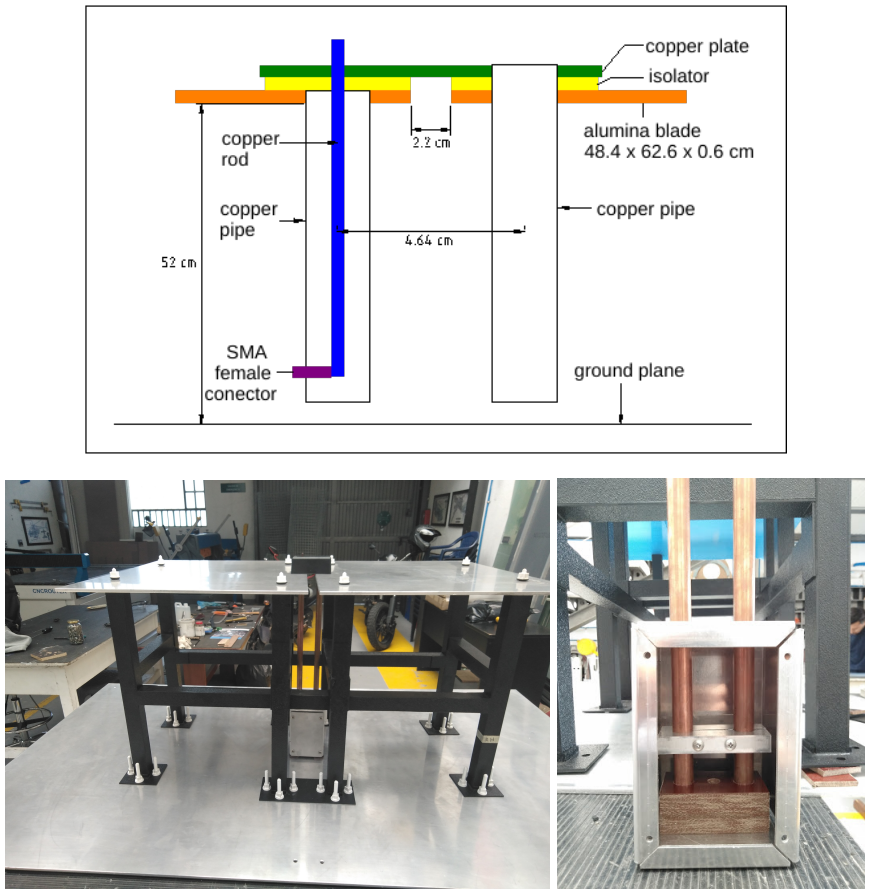

Note. Schematic of the antenna (top), image of the blade antenna (bottom left) and closeup of the balun tuner (bottom right).

2.2. Software Defined Radio (SDR)

Software Defined Radio (SDR) is an upcoming technology initially designed for radio-communication purposes. Essentially, it is a re-programmable and re-configurable device for analogical and digital applications. It has three main stages: a wireless architecture, radio component (hardware), and software component. The main difference with traditional communication platforms is that they can control parameters such as center frequency, bandwidth, amplification, and

Figure 6
Schematic of the Roberts Balun.

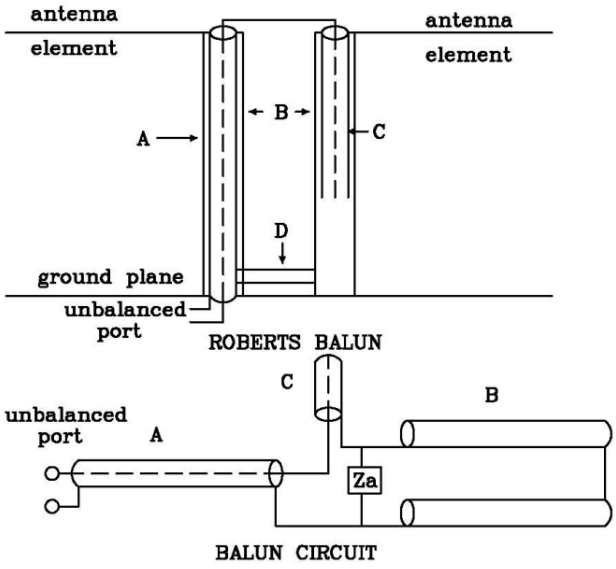

Note. Adapted from Roger (2012).

data sample by software configuration (Arnold, 2020). There have been applications for radio astronomy using this kind of technology. Among them are: testing of different SDRs for radioastronomy and RFI detection purposes (Keller et al., 2015), an SDR optimized for radio astronomy (Vacaliuc et al., 2012), an SDR-based low-frequency array for the observation of the Deuterium hyperfine line at 327.4 MHz (Ragoomundun and Beeharry, 2019), and the development of an SDR ground-based system for interferometric radar (Feng et al., 2021). It is worth noting that SDR technology has not yet been used for this particular scientific case.

An ideal SDR architecture would have a Digital to Analog Converter (DAC), and an Analog to Digital converter (ADC) connected directly to the processor and antennas; this would provide autonomy for the processor to handle signal processing exclusively (Saptarshi, 2018). However,

this is not technologically possible (see Figure 7 left), resulting in stages assumed by a transceiver and an FPGA (see Figure 7 right); for our application the Tx stage is not used, only the Rx stage. The LimeSDR family allows reconfiguration of per-channel parameters such as carrier frequency, low-pass filter, latency factor, and buffer control in the FPGA.

Figure 7
General SDR architecture

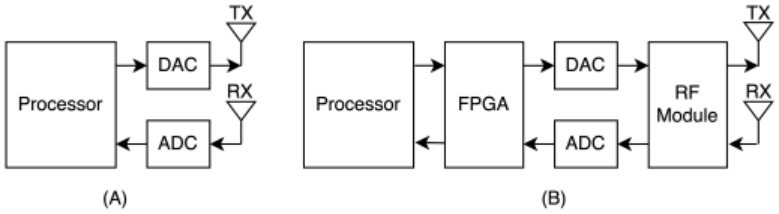

Note. Block diagram of an ideal SDR (left) and a typical SDR architecture (right). Adapted from (Saptarshi, 2018).

2.2.1. Limenet mini. A Limenet mini net is an IoT platform that contains a mainboard (Processor: Intel Core i7-7500U, two cores, 2.7 GHz (3.5 GHz boost)), memory (32 GB 2 x 16 GB SO-DIMM DDR4 2133 MHz), storage (512 GB SSD), 4 USB ports, 1 GigaByte Ethernet port and 5 antenna ports. This is a MIMO device with 3 sma ports for Rx and 2 for Tx. The mainboard contains FPGAs, RF transceivers, internal memory, USB controllers, and oscillators. It operates in a frequency range between 100 kHz to 3.8 GHz (Limenet micro web page).

2.2.1.1. LimeSDR-USB board. The Limenet mini radio is a LimeSDR USB micro Type-B. An image of the top view highlighting its principal components is illustrated in Figure 8 and LimeSDR-USB features and specifications are pŕesented in Table 2.

In reception mode, the signal enters through one of the female SMA connectors, passes through a coupling stage, and is introduced to the Transceiver. Then it goes to the FPGA through

Figure 8
LimeSDR-USB board

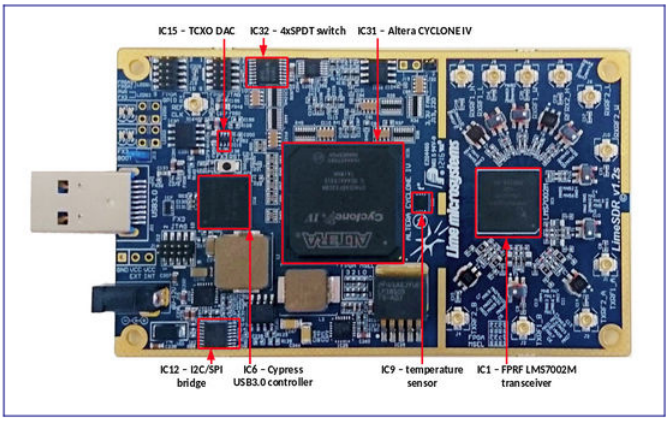

Note. Upper view of the LimeSDR-USB board highlighting the main components. Adapted from Lime Microsystems manual.

the USB 3.0 peripheral control stage and then to the USB connector, which allows the connection to a computing unit. The architecture of the LimeSDR-USB board is presented in Figure 9.

Internally, the LimeSDR-USB has an LM7002M FPRF Transceiver. The LMS 7200 LNA gain stage ranges between 30 and 32 dB (1 and 3 dB steps), the noise figure is 2 dB, and the frequency range is between 30 and 3800MHz.

In reception mode, the gain control of the LMS 7200 consists of several stages. First, the signal goes through an amplification stage composed of LNAs, one for each frequency range: Low (LNAL), High (LNAH), and Wideband (LNAW). Then the signal goes through a mixer, and a second amplification stage passes through a low-pass filter, and reaches the final amplification stage if required. At last, the signal reaches the ADC and the Transceiver Signal Processor (TSP) to finally reach a digital IQ interface (port 1 and port 2). The Voltage Controlled Oscillator (VCO) and the amplifiers can be manipulated from LimeSuite or GNU Radio. The ADC samples at a

Figure 9
LimeSDR-USB board architecture

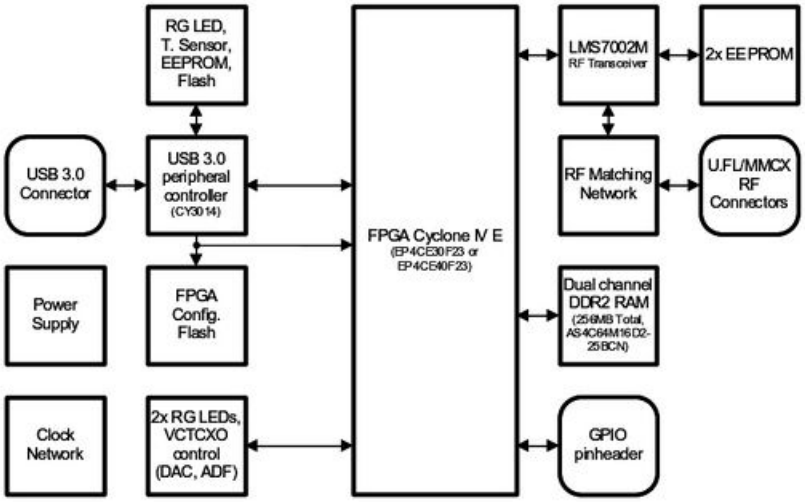

Note. Adapted from Lime Microsystems manual.

rate of 100 MS/s quantized at 14bits/sample. Gain or attenuation values must be modified to use the sampled bits optimally without reaching saturation generated by over-amplification (Saptarshi, 2018). The architecture of the LMS 7200 transceiver is presented in Figure 10.

2.2.1.2. ADC considerations. Nyquist theorem proposes that if a continuous signal has a bandwidth BW, it can be sampled at a frequency F greater than or equal to 2 times BW $(FS > 2BW)$. If the signal passes through a bandpass filter with bandwidth B (or through a Down Converter) BW will be equal to $B/2$, resulting in $FS > B$. The LimeSDR ADC measures, in discrete time, the voltage of a signal separated by a time T. The measurements are linked to a sampling frequency $Fs = 1/Ts$. From the Nyquist theorem, the sampled signal can reach a maximum frequency expressed as the quotient of Fs (sampling frequency) over 2 $(F_{max}/2)$, so an ADC has limitations in its bandwidth. The quantization process is a type of amplitude sampling.

Table 2
LimeSDR-USB specifications.

Component	Description
Board	LimeSDR USB micro Type-B
Antennas	Five (of which one is dedicated for HF reception)
Cables	5 ×U.FL (internal and pre-installed)
RF Transceiver	Lime Microsystems LMS7002M MIMO FPRF
FPGA	Altera Cyclone IV EP4CE40F23
Memory	256 MBytes DDR2 SDRAM
USB 3.0 controller	Cypress USB 3.0 CYUSB3014-BZXC
Oscillator	Rakon RPT7050A @30.72MHz
Continuous frequencyrange	100 kHz – 3.8 GHz
Bandwidth	61.44 MHz
RF connection	10 U.FL connectors (6 RX, 4 TX)
Power Output	(CW) up to 10 dBm
Multiplexing	2×2 MIMO
Power	Micro USB connector
Status indicators	Programmable LEDs
Dimensions	100 mm × 60 mm

Note. Adapted from LimeMicrosystems manual.

This process is closely linked to sampling, expect it is non-reversible (Ortega and Reyes, 2020). At the output of the ADC, there is a number bounded by bits, for example, 32 bits/sample or 64 bits/sample.

An ADC has lower and upper limits depending on the amplitude of the delivered signal regarding the original one (quantization diapason). Among the disadvantages of using ADC is the deformation of weak waves due to the quantization process since it is expressed with few amplitude levels (Saptarshi, 2018).

Figure 10
Block structure of the LMS7002M transceiver

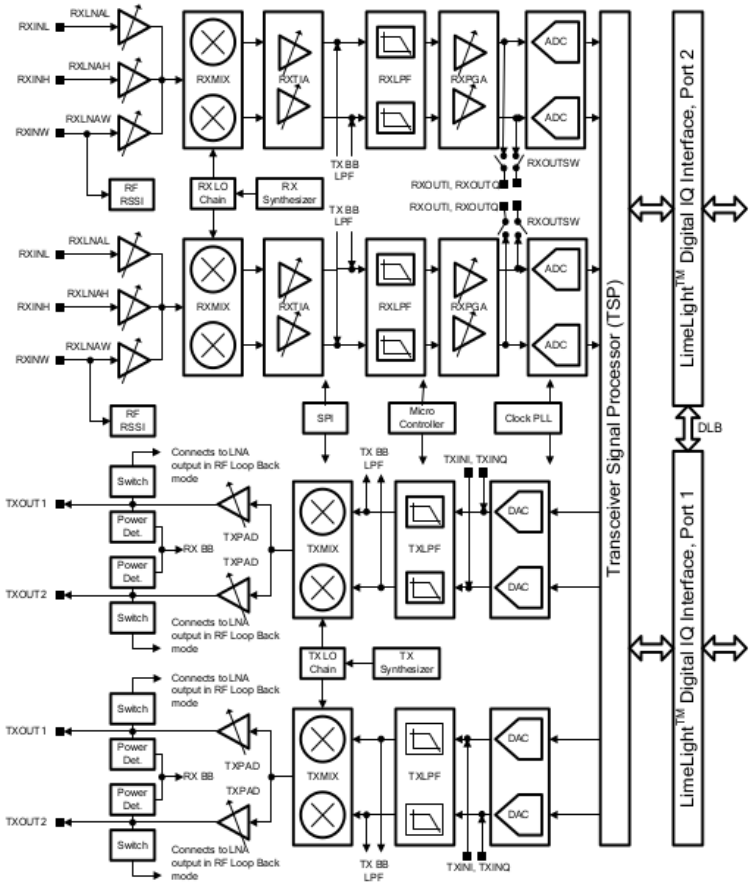

Note. Adapted from LMS7002M datasheet.

2.3. Software architecture

The implemented software architecture uses GNU Radio for the SDRs configuration and the definition of the data pre-processing.[2] First of all, it was implemented a block diagram containing

[2] The algorithms were developed by Ronal Sebastian Buitrago Parra, Yeison Andrés Quiroga Malambo, Brayan Nicolas Suarez Mongui and Felipe P. Mosquera.

LimeSuite and USRP source blocks and a frequency sink. From this diagram, a Python (.py) file is created with the codification of the used blocks. A binary file (.bit) with the data is generated using a file sink block.

Two software packages were made, one for use with the Limenet mini (lime_eor) and the other for the Ettus E310 (etus_eor). Each main folder contains the same file structure but is configured for each SDR. Taking the Ettus folder as an example, it contains three files with .py extension and two folders, ”data” and ”graphics”. Figure 11 shows a diagram of the implemented software architecture.

The three .py files used are python_graficas_2.py, tomaDatosRFI.py, and tomaDatosRFI.py.

- python_graficas_2.py: is the file generated by GNU from the implemented block diagram.
- dataGNU.py: from the file python_graficas.py this file extracts the center frequency, which in this case is 108 MHz. The samp rate is also defined, which in our case is 16 Ms/S equivalents to obtain 16 MHz display windows and a FFT size of 6144. This file invokes and reads the binary .bin file and generates the plots. The .bit file is invoked in this file, and the values are converted to vectors using numpy. Then, the vector length is calculated, and the size of the power data corresponding to the y-axis is assigned. Next, the operating frequencies and limits for the display window are defined. Then the x-axis increment or steps are defined, and a vector that fills and organizes the data packets is defined; it is converted to a vector array (numpy). Subsequently, the graphing is performed where the central frequency and the limits on the x and y axes are defined and located, and the number of display windows is

assigned.

- tomaDatosRFI.py: takes the GNU data and iterates six times, varying the center frequency to cover the range of 100 to 200 MHz. It extracts the dates and times of the data and generates the files that feed the graphs and data folders. In lines 24 to 45 of this file, the file path must be defined according to the location of the root folder used, e.g., to install and compile the software from any Linux device. When compiling this file, six graphs are generated in .jpg format. Each of these graphs corresponds to a different frequency window: from 100 to 116 MHz, 116 to 132 MHz, 132 to 148 MHz, 148 to 164 MHz, 164 to 180 MHz, 180 to 196 MHz, and 196 to 212 MHz. At the end of the data acquisition, it resets the center frequency to 108 MHz to be able to perform new data acquisition. The obtained graphs are organized and classified by subfolders according to the date and time of the data acquisition. The raw data is stored in a .txt file for post-processing procedures. Additionally, an algorithm was generated (multiplesTomasRFI.py) to define the number of measurements and their separation in time (sg).

Figure 11
Software architecture using GNU Radio.

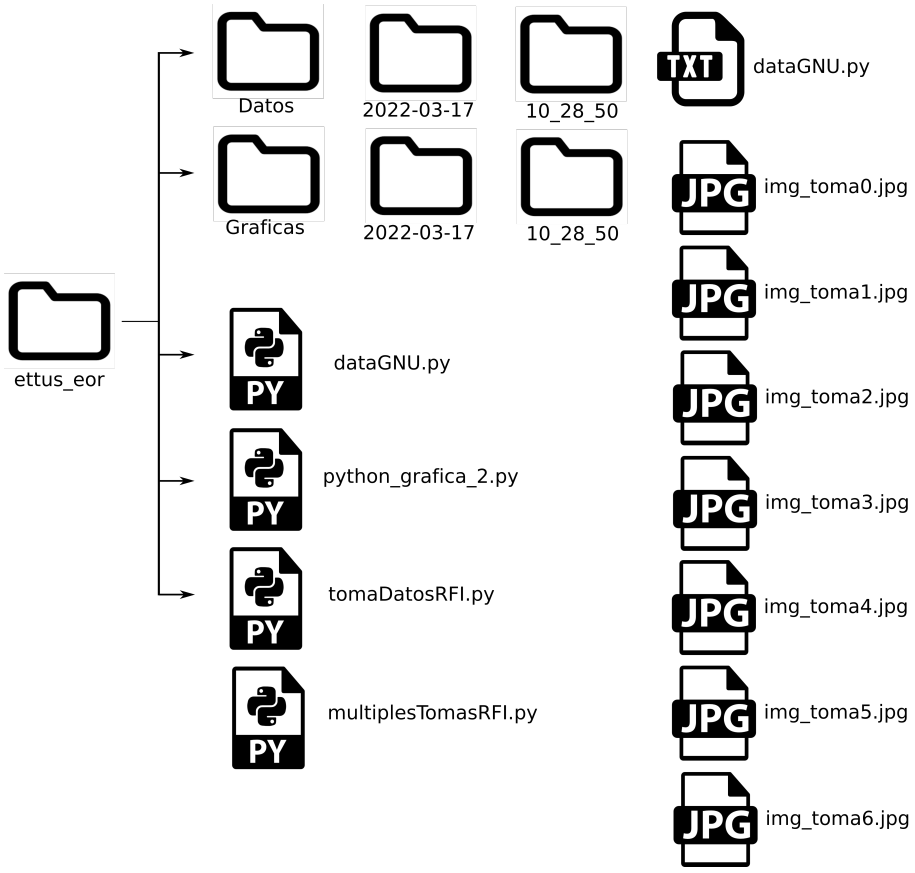

3. Simulations

Simulations of the blade antenna were performed using Ansys High-Frequency Structure Simulator (HFSS) and python algorithms compiled in the Spyder platform of Anaconda (co-simulation) (Restrepo et al., 2020). The simulation procedure included several phases. First, initial parameters were assigned to define the geometries of the antenna parts and to assign values required for the simulation (frequency, dimensions of the radiation box).

The characteristics of the antenna simulations are presented in Table 3.

Table 3
Specifications and parameters of antenna simulations.

Antenna	Frequency (MHz)	Software	Parameters
Blade	100-200	HFSS	S_{11}, chromaticity for planes $\phi = 0°$ and $\phi = 90°$, and bandwidth (BW)

For the simulations antenna, the dimensions used in the actual antenna were used as reference: dipole = 48.8 x 62.6 cm, dipole thickness = 6 mm, gap between dipoles = 2.2 cm and dipole height = 52 cm.

Three main parameters were considered to analyze the antenna's behavior: S_{11} parameter response, chromaticity (gain change for plane $\phi = 0°$ and gain change for plane $\phi = 90°$) , and normalized gain. The simulations obtained from the S_{11} parameter permits inferring the antenna bandwidth through the inspection of reflected waves. The signal wave range with values less than

-10dB [3]establishes the antenna's bandwidth or frequency operating range. The simulations of the gains for planes $\phi = 0^\circ$ and $\phi = 90^\circ$ were used to obtain the chromaticity plots.

3.1. S_{11} parameter simulations

The S_{11} simulations will be used to compare them with the measurements performed to the antenna. From these simulations, it is possible to obtain the bandwidth and center frequency of the antenna and have criteria to define the ideal position where the balun tuner should be placed; the balun description and function is presented in section 2.1 Blade Antenna.

Figure 12 illustrates the behavior of the blade antenna iterating between different positions of the balun tuner. These positions, expressed in centimeters, represent the balun tuner height referenced to the lower level of the balun. Five positions or heights were evaluated: 7.5, 12.5, 22.5, 32.5 and 42.5 cm. The analysis is performed between 100 and 200 MHz (see Table 4).

Table 4
Blade antenna S_{11} parameter simulations (different balun heights)

Concept	7.5cm	12.5cm	22.5cm	32.5cm	45.5cm
Minimum frequency @-10dB (MHz)	100	100	100	100	142
Maximum frequency @-10dB (MHz)	141	144	152	164	196
Bandwidth (BW) (MHz)	41	44	52	64	54
Minimum gain (dB)	-19.58	-21.23	-27.50	-47.14	-26.98
Frequency @ min. gain (MHz)	117	118	124	135	163

A frequency shift trend is seen when increasing the tuner height. As the height of the

[3] The -10 dB criteria is widely used in telecomunications. The S11 parameter, applied for antennas measurements, establishes the power delivered to an antenna as the power reflected by impedance mismatch and is defined as $1/\sqrt{dB(level)}^2$. In this case assuming a value of -10 dB the result of the losses is 0.1 which is optimal to establish the performance of the antenna.

balun increases, the frequency response shifts towards higher frequencies. The best response as a function of balun tuner height is found at the 22.5 and 32.5 cm positions when evaluating the response of the criteria mentioned above.

Figure 12
S_{11} simulation (antenna 1:1)

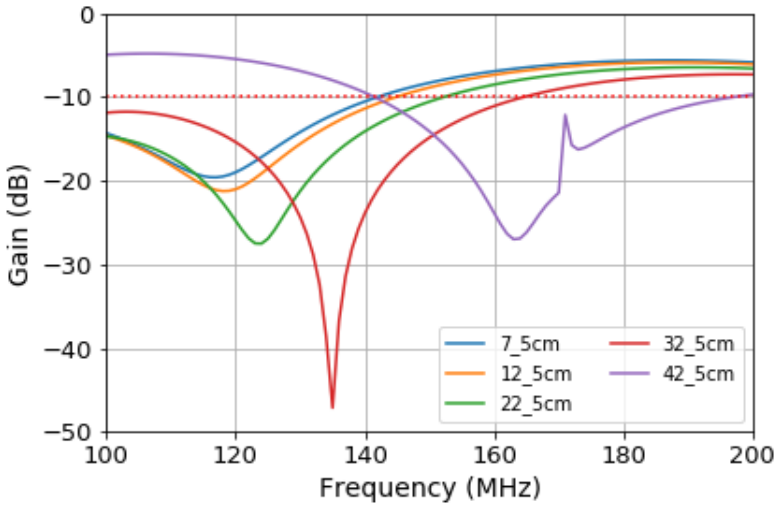

Note. Comparative of S_{11} simulations for the 1:1 antenna considering 5 balun positions. Ansys HFSS license from Universidad de Chile.

3.2. Chromaticity

Results of the chromaticity simulations for the 1:1 balun antenna for $\phi = 0°$ and $\phi = 90°$ are presented in Figure 13. To obtain the chromaticity, three plots were produced: gain, gain interpolated and gain change. Chromaticity in an antenna expresses the level of gain variation as a function of frequency and angle. Simulations were performed for the blade antenna locating the balun at 22.5cm. The criteria to locate the balun at that height was that considering the comparison of the simulations vs. measurements (see section 5 Results) the best fitting was achieved at 22.5cm. Using HFSS, gain simulations were performed for planes $\phi = 0°$ and $\phi = 90°$. Subsequently, these

.csv files were processed by a Python code (developed by Restrepo and Lucero. U. of Chile) which runs routines for data processing and converts them into the observed graphical representation.

For the plane $\phi = 0°$, the minimal gain variation was found between 140 and 150 MHz. Two zones of considerable gain change were found in the regions between 0 and 40 degrees in frequency ranges of 100 to 130 MHz and between 160 and 200 MHz. From 60 degrees onward, the gain change for all frequencies is minimal.

Regarding the gain variation as a function of frequency for plane $\phi = 90°$, a minimum variation was found between 118 and 143 MHz. There is a high positive variation of gain between 100 and 118 MHz between 0 and 40 degrees and a negative variation between 185 and 200 MHz between 0 and 20 degrees. As observed for plane $\phi = 0°$, it is found that the antenna response is optimal for angles greater than 60 degrees since there is a minimal gain variation for that range.

Figure 13

Chromaticity simulation (blade antenna)

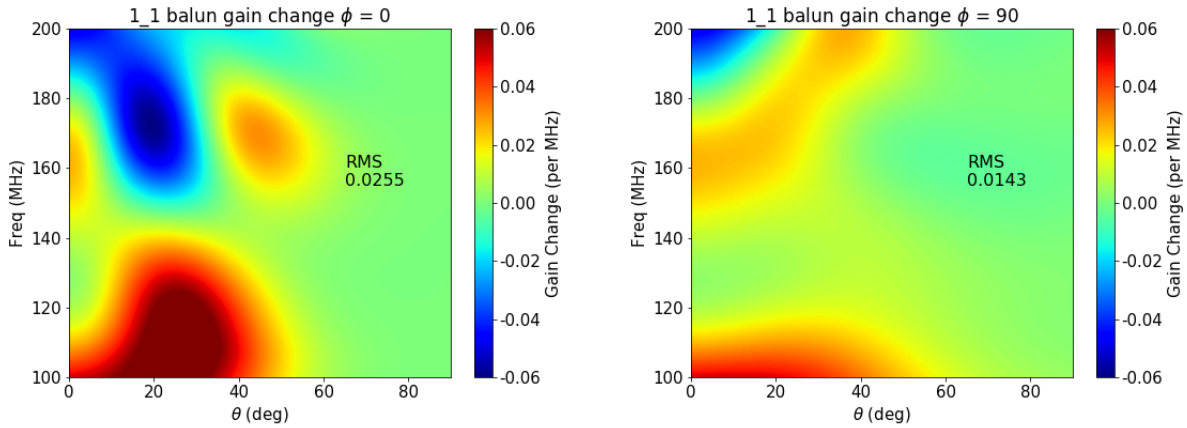

Note. Blade antenna chromaticity @ 22.5 cm. gain change for planes $\phi = 0$ (left) and $\phi = 90$ (right). Ansys HFSS license from Universidad de Chile.

4. Measurements

In this section are presented the following items: VNA antenna measurements of S_{11} parameter, SDRs sensitivity and linearity measurements and Pre-amplifier LNAs S_{21} measurements.

4.1. VNA antenna measurements of S_{11} parameter

The blade antenna was measured in-situ using a portable VNA. The measurements were performed in the Paramo de Berlin, using a Fieldfox N99-14A Portable VNA with frequency ranges between 30 kHz and 6.5 GHz was used. Measurement specifications are defined in Table 5.

Figure 14
UIS dipole-blade 100-200 MHz antenna

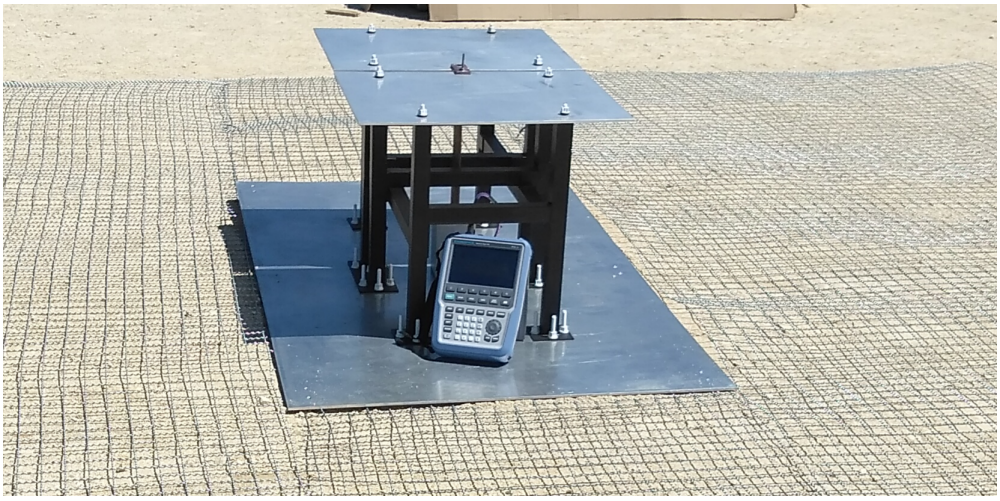

Table 5
Specifications and parameters of antenna measurements.

Antenna	Frequency (MHz)	Location	Instrument	Parameters
Blade	100-200	in-situ	VNA Fieldfox N99-14A (30 kHz-6.5 GHz)	S_{11} and bandwidth

Table 6

Blade antenna S_{11} parameter measurements (different balun heights)

Concept	7.5cm	12.5cm	22.5cm	32.5cm	45.5cm
Measurement min. freq. @-10dB (MHz)	112	112	111	111	117
Measurement max. freq. @-10dB (MHz)	145	149	158	166	179
Measurement BW (bandwidth) (MHz)	33	37	47	55	62
Measurement min. gain (dB)	-15.81	-16.50	-19.72	-41.91	-28.45
Measurement frequency @ min. gain (MHz)	126	124	124	126	161

Figure 15

S11 measurement (antenna 1:1)

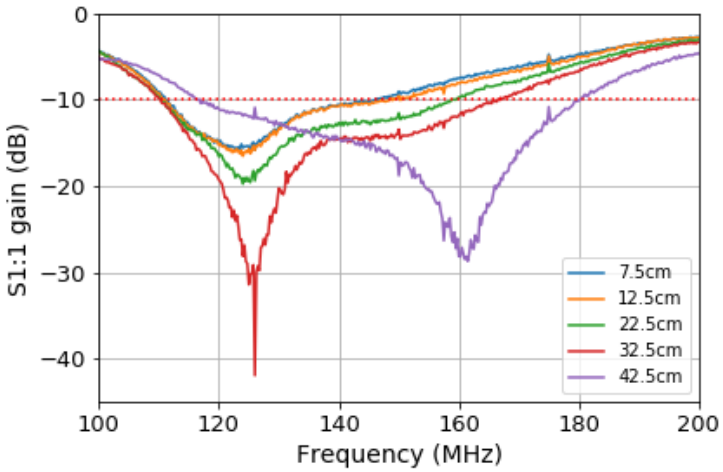

Note. 1:1 antenna S11 parameter VNA measurements considering different balun tuner heights.

The measurements of the blade antenna 14 were performed in-situ using a portable VNA. As mentioned in section 2.1, the 100-200 MHz antenna is a dipole-blade with balun. For balun tuner positioning, five heights were considered (7.5, 12.5, 22.5, 32.5, and 42.5 cm). Due to the presence of the SMA port on the antenna, the minimum balun tuner height is 7.5 cm. The frequency range for -10 dB levels, bandwidth, minimum gain level, and the respective frequency for that level are analyzed. Figure 15 illustrates the S11 response of the blade antenna considering different balun positions and in Table 6 are presented the results of the measurements.

4.2. SDRs sensitivity and linearity measurements

Parameterized signals were injected to measure the performance and response of the SDRs (Limenet mini, Ettus E310 and USRP 2920). A Rhode Schwarz ZVL6 VNA in spectrum analyzer mode with a range between 9 kHz and 6 GHz was used to obtain the reference of the SDR measurements. To inject signals to the SDRs a Marconi Instruments was used as a signal generator with an operating range between 9 kHz and 1.2 GHz. With this equipment, signals were injected into the receivers, varying frequency and RF levels (amplitude). Preliminary tests were performed using an oscilloscope to validate the signal generator's correct behavior and establish a reference for the upcoming SDR measurements. In these tests, signals were injected directly from the signal generator to the oscilloscope varying frequencies and RF levels, checking the correct calibration of the generator.

Figure 16
Setups for SDR measurements.

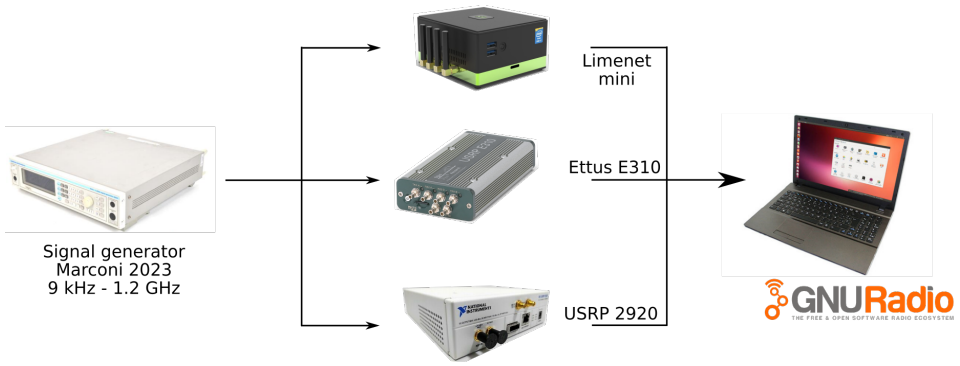

Note. Images: www.ettus.com/all-products/e310/, www.ebay.com/itm/282506896648, www.artisantg.com/TestMeasurement/69602-1/Cobham-Aeroflex-Marconi-2023A-9-kHz-to-1-2-GHz-Signal-Generator, www.limemicro.com and www.gnuradio.org

Two types of measurements were established to evaluate the performance of the SDRs.

The first set of measurements was oriented to obtain the linearity of the SDRs by maintaining an injected level of -30 dBm and varying the frequencies between 100 and 200 MHz considering 1 MHz steps. Measurements were performed configuring the SDRs with a gain of 0 dB. The second set of measurements sought to establish the SDRs sensitivity levels. A signal with a fixed frequency of 150 MHz was injected, varying the RF levels between -30 and -120 dBm. The SDRs were configured with gains between 0 and 60 dB.

Tests were complemented by using processing blocks in Gnu Radio, to configure each SDR and obtain the response for each test. Values were assigned for the following parameters: sample rate = 1 MS/s (1e6), fft size = 1024*8 (8192k), freq min = 100 MHz, freq max = 200 MHz, steps = 1 MHz, NCO frequency = 0, CHB calibration bandwidth = 5 MHz, CHB analog filter bandwidth = 5 MHz, CHB digital filter bandwidth = 0, Y-axis min = -140 and Y-axis max = 10 Interactive plots of frequency (MHz) vs. gain (dB) were generated when compiling the GNURadio block diagram. Figure 28 illustrates one of the data acquisition procedures where a signal peak level of -61.74 dB at 150 MHz is seen.

4.2.1. SDRs linearity. As mentioned above, the first set of measurements sought to establish the linearity response of the SDRs by varying the injected frequencies (between 100 and 200 MHz) and maintaining the same RF level (-30 dB). These measurements were performed by configuring the SDRs with a gain of 0 dB which is the gain value used for the initial sky measurements. A reference level was established by the obtained response of a VNA in spectrum analyzer mode.

Figure 18 shows that the VNA in spectrum analyzer mode response is stable at the -30 dB

Figure 17
Screenshot from a SDR measurements.

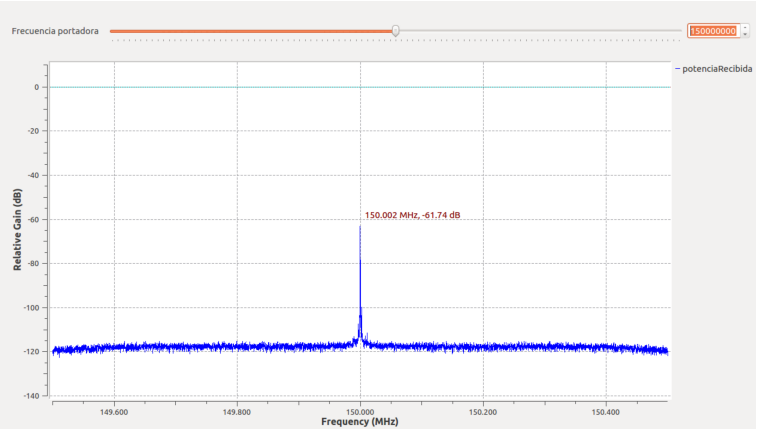

level at these frequencies. The variations in gain achieved by the spectrum analyzer are −30.4 dB @100 MHz and −30.43 dB @ 200 MHz. The response of the Limenet mini exhibits a gain variation between −67.45 dB @ 100 MHz and -60.06 dB @ 200 MHz. For the Ettus E310 a variation between −47.78 dB @ 100 MHz and −45.59 dB @ 200 MHz was obtained. As for the response of the USRP 2920, a gain variation between −27.45 dB @ 100 MHz and −45.59 dB @ 200 MHz was observed.

4.2.2. SDRs sensitivity. Figure 19 plots the response of the SDR when injecting a signal with a fixed frequency of 150 MHz, varying the RF level from −30 to −130 dBm with 10 dBm steps, configuring the SDRs receivers with gains between 0 and 60 dB.

A noise floor of -78.39 dB was found for the Limenet mini. When injecting signals between −30 and −130 dB, and configuring the Limenet at gain 0, no response is found at levels lower than −50 dB i.e. the injected signal does not exceed the noise floor. At higher levels, the injected signal exceeds the noise floor. For an SDR gain of 10 dB, the response is obtained from −60 dB, for 20

Figure 18
SDRs linearity response

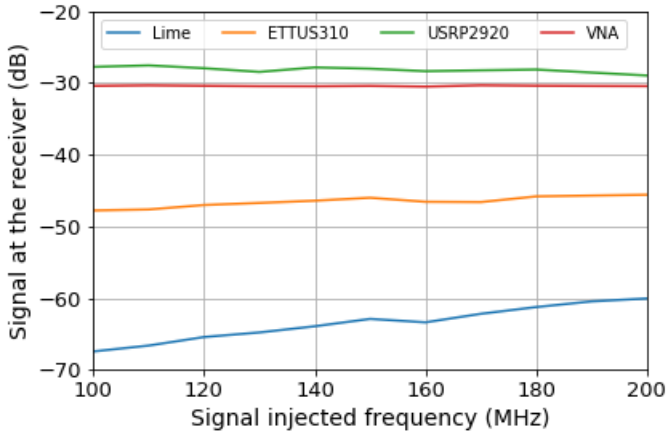

Note. Limenet mini, Ettus E310 and USRP2920 linearity response @ gain=0, injecting -30dBm and varying the frequency between 100 and 200 MHz.

dB from −70 dB, and 30 dB from −80 dB. The behavior observed when configuring the SDR at 40, 50, and 60 dB is similar, appreciating response in injected signals higher than −90 dB.

As for the Ettus E310, configured with a gain of 0 dB, a response is observed from an injected signal of -90dB. When configured with a gain of 20 dB, the response is obtained from −100 dB and for 30 dB from −110 dB. For receiver gains of 40, 50, and 60 dB the response is obtained from signals below −120 dB.

When configuring the USRP 2920 at 0 dB, the response is obtained from −110 dB and at 10 dB gain from −120 dB. When configured with 30 dB gain, a response is obtained from the minimum injected level corresponding to -130 dB. The responses at 40, 50, and 60 dB are identical; superimposed results are shown for these levels.

Figure 19
SDRs sensitivity response

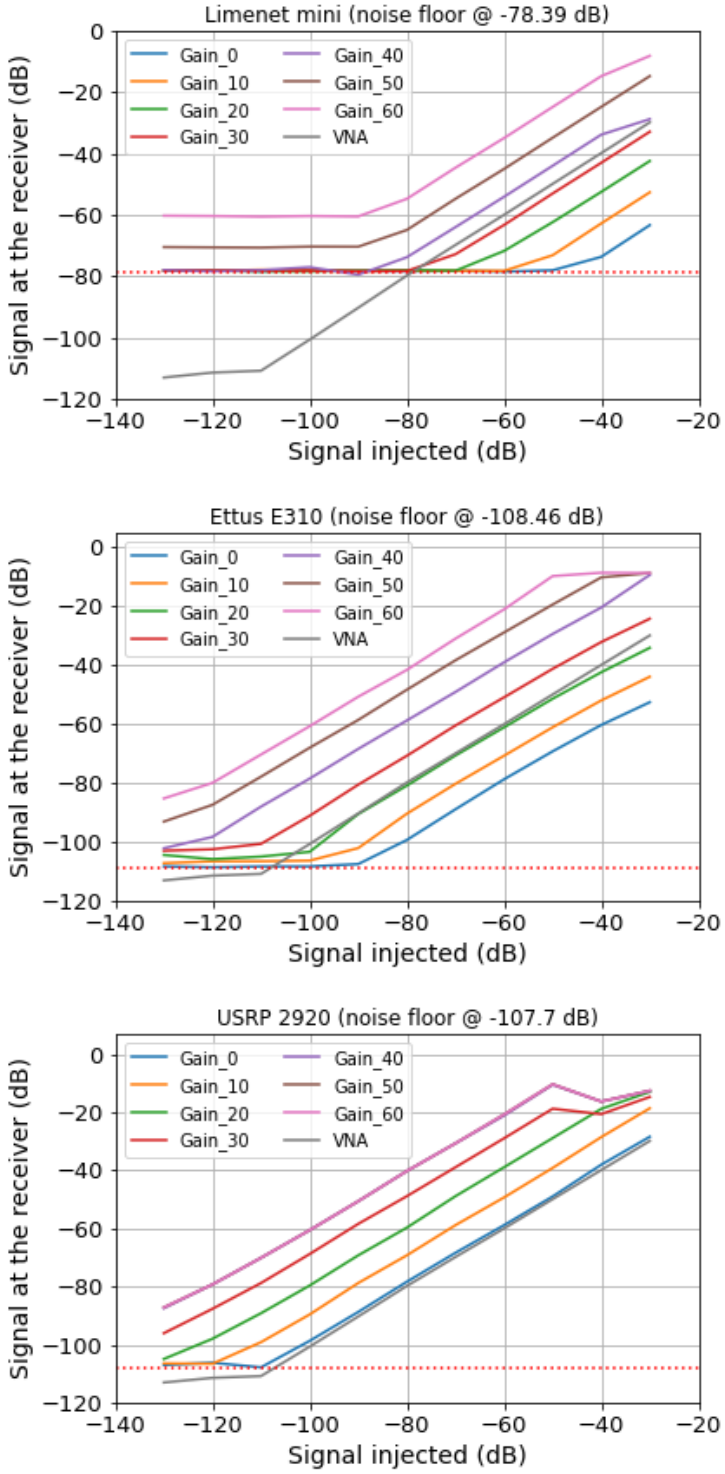

Note. Limenet mini (top), Ettus E310 (middle) and USRP2920 (bottom) sensitivity response @ SDR gain = 0, injecting 150 MHz and varying the RF level between −30 and −120 dBm.

4.3. Pre-amplifier LNAs S_{21} measurement

S_{21} measurements were performed to establish the response of the current preamplifier LNAs (model ZX60-P103LN+). Figure 20 (left) shows the response for one LNA and in Figure 20 (right) for two coupled LNAs. The actual preamplifier uses two coupled LNAs. The performed measurements of a single LNA and two-coupled LNAs were done to verify the response of such devices.

Figure 20
Pre-amplifiers LNA S_{21} response

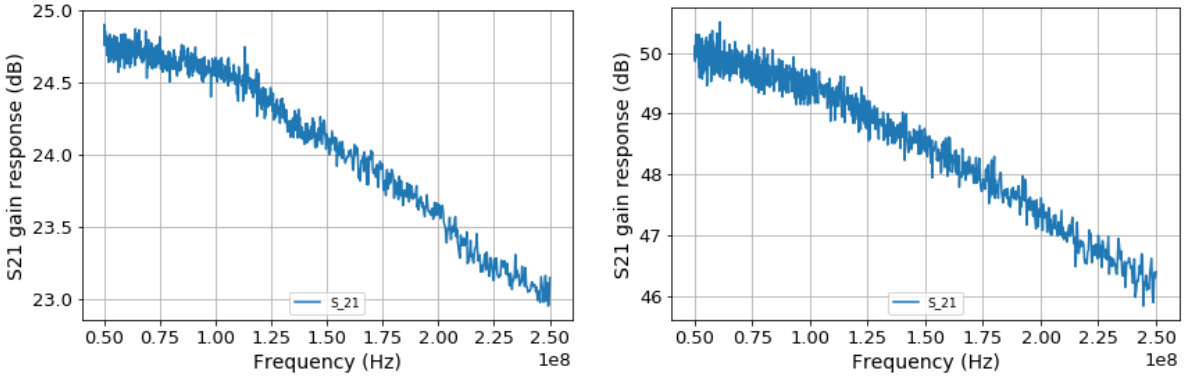

Note. S_{21} response of the current pre-amplifier LNA ZX60-P103LN+, testing one LNA (left) and testing two-serial LNAs (right).

The S_{21} measurements performed on the LNA show a decremented behavior in terms of gain response as a function of frequency. A single amplifier obtained a gain of 24.76 dB at 50 MHz and 24.72 dB at 75 MHz. When evaluating the performance at 100 MHz, there is a narrow decrease compared to 50 and 75 MHz, obtaining a gain of 24.54 dB. From 125 MHz, the response slope is steeper, i.e., the gain decreases with a higher rate. The measurements for higher frequencies are 24.43 dB at 125 MHz, 24.08 dB at 150 MHz, 23.92 dB at 175 MHz, 23.06 dB at 200 MHz, and

23.14 dB at 250 MHz.

As for the measurements made to the two coupled LNAs, a similar response was achieved as expected. For 50 MHz, a gain of 49.92 dB was obtained, and for 75 MHz, 49.636 dB. From 100 MHz onward, as in the case of the single amplifier measurements, a response with a steeper slope is observed. At 100 MHz 49.56 dB was obtained, at 125 MHz 48.95 dB, at 150 MHz 48.37 dB, at 175 MHz 47.92 dB, at 200 MHz 47.61 dB and at 250 MHz 46.4 dB. These measurements show a differentiated behavior in terms of LNA gain response for each frequency.

5. Results

The results obtained from the simulations and measurements are presented below. Initially, the calculations of the effective area of the antenna as well as the source temperature (sun) are mentioned. Next, the procedures to establish the total temperature and the system's noise figure are shown. These calculations are based on three scenarios determined by the pre-amplifier configurations.

5.1. Effective area

Considering an antenna gain of 7 dB [4] and a central frequency of 150 MHz, the effective area of the blade antenna is:

$$A_e = \frac{\lambda^2 G}{4\pi} = \frac{(\frac{3*10^8}{124*10^6})^2 * 7}{4\pi} = 3.2605 m^2$$

5.2. Source temperature

The sun was chosen as the cosmic reference source because it is a well-studied source that allows us to know the flux intensity accurately. The flux of the sun is:

$$1.24 * 10^6 Jy = 1.24 * 10^{-20} \frac{W}{m^2 Hz}$$

[4] This value was obtained based on the blade antenna gain simulation.

the source temperature is then:

$$T_{src} = \frac{A_e}{2k} S_v = \frac{1.7905}{2k} 1.24 * 10^{-20} = 1464.1737K$$

5.3. Total system temperature

The deduction of the system temperature was made considering three scenarios: not using a pre-amplifier, using the current preamplifier, and using the suggested pre-amplifier. For all scenarios, a standard antenna temperature was considered. The antenna temperature T_{ANT} was defined taken as reference the International Telecommunications Union recommendation UIT-R P.372-7 for the antenna temperature characterization (see Figure 21). At 200 MHz we define an antenna temperature of 300 K.

Figure 21
ITU reccomendation

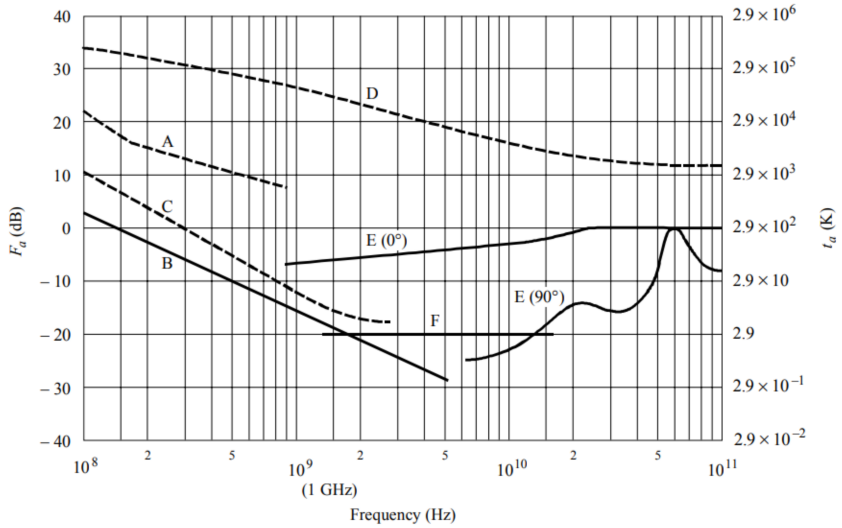

Note. ITU-R P.372-7 radio noise recommendation. Where A is the estimated media of man-made noise, B is the galactic noise, C is the galactic noise toward galactic centre, D is the quiet sun, E is the atmospheric disturbances and F cosmic background noise level (2.7 K)

5.3.1. System temperature without pre-amplifier. The system's temperature without a preamplifier was calculated to have reference levels against which to compare both the current and the suggested preamplifier. A 100 ft. long LMR400 cable was considered for connecting the antenna and the receiver. Figure 22 illustrates a conceptual diagram of the subsystems to calculate the overall temperature of the system. In this case, no pre-amplifier was considered. The following parameters were taken into account: component, reference of the component, gain expressed in dB, linear gain, noise figure in dB, and system temperature expressed in Kelvin (see Table 7).

Figure 22
Front-end block diagram (without pre-amplifier)

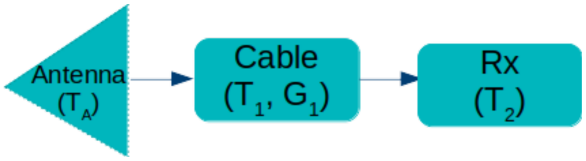

Note. Diagram of the subsystems to calculate the overall temperature of the radio telescope without pre-amplifier.

Table 7
System temperature estimation parameters (without pre-amplifier)

Component	Reference	G(dB)	G(linear)	NF(dB)	T(K)
cable (T_1, G_1)	LMR400 × 100 ft	-1.5	0.993	1.5	119.36
receiver (T_2)	Ettus E310	–	–	8	1539.776

Note. Gains (in dB and linear), noise figure and temperature per subsystem (without pre-amplifier)

Considering those values the temperature of the subsystems is:

$$T_{RX} = T_1 + \frac{T_2}{G_1(linear)}$$

$$T_{RX} = 119.36 + \frac{1539.776}{0.993} = 1669.9904K$$

The overall system temperature is defined as $T_{SYS} = T_A + T_{RX}$ obtaining:

$$T_{SYS} = 300K + 1669.9904K = 1969.9904K$$

The subsequent Noise figure NF isand the Noise Factor (F) is:

$$NF = 8.917dB$$

$$F = 7.79$$

By analyzing the results, the system presents extremely high noise values, expressed by elevated temperatures found both for the antenna receiver (T_{RX}) and the integrated system (T_{SYS}). Table 8 presents the results of the calculations for the system, considering that T_{REF} is the temperature of the receiver (all stages except the antenna), T_{ANT} is the temperature of the antenna, T_{SYS} is the temperature of the system, NF the noise figure, and F the noise factor.

5.3.2. System temperature with current pre-amplifier. The current preamplifier consists of two Mini-Circuits ZX60-P103LN+ low noise amplifiers and a Mini-Circuits ZFBT-4R2GW-FT+ bias tee. Two types of cables were considered. For the connection between the antenna and the bias tee, a low loss sma cable (female-female) was used, and for the connection between the second LNA and the receiver, an LMR400 coaxial cable. The LMR400 distance of

Table 8
System temperature and noise figure results (without pre-amplifier)

Parameter	Value
Antenna Effective area	1.7905m^2
Source temperature (sun)	804.0779K
T_{RX}	1669.9904 K
T_{ANT}	300 K
T_{SYS}	1969.9904 K
NF	8.917 dB
F	7.79

Note. Temperatures (RX, antenna and system) and noise (figure and factor) results (without pre-amplifier)

100 feet was used to project the system for future applications. Figure 23 presents a schematic of the current pre-amplifier stages and Table 9 illustrates the following parameters: component model, gain (linear and in dB), noise figure (dB), and temperature (K).

Figure 23
Front-end block diagram (current pre-amplifier)

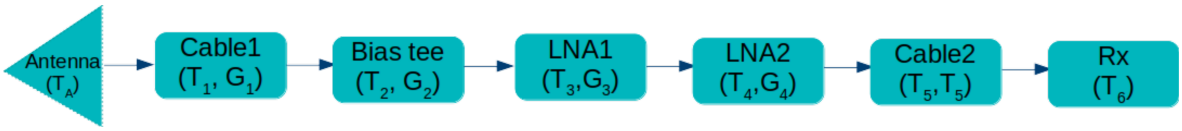

Note. Diagram of the subsystems to calculate the overall temperature of the radio telescope considering the current pre-amplifier.

According to the Friss temperature equation T_{RX} is:

$$T_{RX} = T_1 + \frac{T_2}{G_1} + \frac{T_3}{G_1 G_2} + \frac{T_4}{G_1 G_2 G_3} + \frac{T_5}{G_1 G_2 G_3 G_4} + \frac{T_6}{G_1 G_2 G_3 G_4 G5}$$

$$T_{RX} = 2.01 + \frac{42.96}{0.993} + \frac{92.29}{0.993 \times 0.871} + \frac{92.29}{0.993 \times 0.871 \times 199.526} +$$

$$\frac{119.636}{0.993 \times 0.871 \times 199.526 \times 199.526} + \frac{1539.776}{0.993 \times 0.871 \times 199.526 \times 199.526 \times 0.993} = 153.27K$$

Table 9
System temperature estimation parameters (current pre-amplifier)

Component	Reference	G(dB)	G(linear)	NF(dB)	T(K)
Cable1 (T_1, G_1)	086-2SM+ $\times$ 2 in	-0.03	0.993	0.03	2.01
Bias tee (T_2, G_2)	ZFBT-4R2GW-FT	-0.6	0.871	0.6	42.96
LNA1 (T_3, G_3)	ZX60-P103LN+	23	199.526	1.2	92.92
LNA2 (T_4, G_4)	ZX60-P103LN+	23	199.526	1.2	92.92
Cable3 (T_5, G_5)	LMR400 $\times$100ft	-1.5	0.993	1.5	119.36
Receiver (T_6)	Ettus E310	–	–	8	1539.776

Note. Gains (in dB and linear), noise figure and temperature per subsystem (current pre-amplifier)

The temperature of the system T_{SYS} is:

$$T_{SYS} = 300K + 153.27K = 453.27K$$

the noise figure NF is:

$$N_F = 4.09dB$$

and the noise factor F is:

$$F = 2.56$$

Table 10 presents the results for the current pre-amplifier in terms of the T_{RX}, T_{ANT}, T_{SYS}, NF, and F; as defined in subchapter 5.3.1.

5.3.3. System temperature with suggested pre-amplifier. The suggested pre-amplifier design and implementation are oriented to reduce the noise temperature of the system. . The design considers two amplification stages complemented with low-pass and high-pass filters. These filters restrict the frequencies adjacent to those of interest (between 100 and 200 MHz)

Table 10
System temperature and noise figure results (current pre-amplifier)

Parameter	Value
Antenna Effective area	1.7905m^2
Source temperature (sun)	804.0779K
T_{RX}	153.27 K
T_{ANT}	300 K
T_{SYS}	453.27 K
NF	4.09 dB
F	2.56

Note. Temperatures (RX, antenna and system) and noise (figure and factor) results (current pre-amplifier)

(see Figure 24). This architecture is based on the pre-amplification stage used in the MIST and MINIMIST projects (Restrepo et al., 2020).

Figure 24
Front-end block diagram (suggested pre-amplifier)

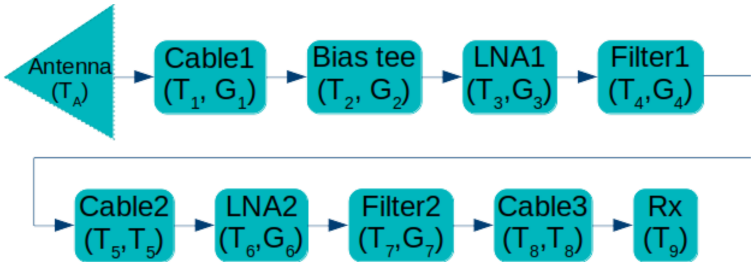

Note. Diagram of the subsystems to calculate the overall temperature of the radio telescope considering the suggested pre-amplifier.

The results of the calculations of the system consider parameters such as gain (expressed in dB and linear), noise figure (expressed in dB), noise factor (dB), and temperatures (K). The values obtained for each parameter are presented in Table 11

According to the proposed design, the temperature of the system is defined by the Friss

Table 11
System temperature estimation parameters (suggested pre-amplifier)

Component	Reference	G(dB)	G(linear)	NF(dB)	T(K)
Cable1 (T_1, G_1)	086-2SM+ × 2 in	-0.03	0.993	0.03	2.01
Bias tee (T_2, G_2)	ZFBT-4R2GW-FT	-0.6	0.871	0.6	42.96
LNA1 (T_3, G_3)	ZX60-33LNR-S+	24.7	295.121	1.1	83.592
Filter1 (T_4, G_4)	SHP-20+	-0.13	0.971	0.13	8.812
Cable2 (T_5, G_5)	086-2SM+ × 2 in	-0.03	0.993	0.03	2.01
LNA2 (T_6, G6)	ZX60-33LNR-S+	24.7	295.121	1.1	83.592
Filter2 (T_7, G_7)	SLP-250+	-0.27	0.94	0.27	18.601
Cable3 (T_8, G_8)	LMR400 ×100ft	-1.5	0.993	1.5	119.36
Receiver (T_9)	Ettus E310	–	–	8	1539.776

Note. Gains (in dB and linear), noise figure and temperature per subsystem (suggested pre-amplifier)

equation arranging the terms as follows:

$$T_{RX} = T_1 + \frac{T_2}{G_1} + \frac{T_3}{G_1 G_2} + \frac{T_4}{G_1 G_2 G_3} + \frac{T_5}{G_1 G_2 G_3 G_4} + \frac{T_6}{G_1 G_2 G_3 G_4 G5} +$$

$$\frac{T_7}{G_1 G_2 G_3 G_4 G_5 G_6} + \frac{T_8}{G_1 G_2 G_3 G_4 G_5 G_6 G_7} + \frac{T_9}{G_1 G_2 G_3 G_4 G_5 G_6 G_7 G_8}$$

and replacing the values:

$$T_{RX} = 2.01 + \frac{42.96}{0.993} + \frac{83.592}{0.993 \times 0.871} + \frac{8.812}{0.993 \times 0.871 \times 295.121} + \frac{2.01}{0.993 \times 0.871 \times 295.121 \times 0.971} +$$

$$\frac{83.592}{0.993 \times 0.871 \times 295.121 \times 0.971 \times 0.993} + \frac{18.601}{0.993 \times 0.871 \times 295.121 \times 0.971 \times 0.993 \times 295.121} +$$

$$\frac{119.36}{0.993 \times 0.871 \times 295.121 \times 0.971 \times 0.993 \times 295.121 \times 0.94} +$$

$$\frac{1539.776}{0.993 \times 0.871 \times 295.121 \times 0.971 \times 0.993 \times 295.121 \times 0.94 \times 0.993} = 142.32K$$

The temperature of the system T_{SYS} is:

$$T_{SYS} = 300K + 142.32K = 442.32K$$

the noise figure NF is:

$$N_F = 4.02dB$$

and the noise factor F is:

$$F = 2.53$$

Table 10 shows the results of the calculations of the system temperature using a pre-amplifier.

Table 12
System temperature and noise figure results (suggested pre-amplifier)

Parameter	Value
Antenna Effective area	1.7905m^2
Source temperature (sun)	804.0779K
T_{RX}	143.32 K
T_{ANT}	300 K
T_{SYS}	443.32 K
NF	4.02 dB
F	2.53

Note. Temperatures (RX, antenna and system) and noise (figure and factor) results (with suggested pre-amplifier)

5.4. Simulations vs measurements

This section is divided into: simulations vs measurements for different balun positions (blade antenna), and SDR measurements comparison.

5.4.1. Simulations vs measurements for different balun tuner positions (blade antenna).

The analysis based on the simulations comparison and the blade antenna measurements considers each balun tuner height. Table 13 illustrates the numeric values of this comparison and in Figure 25 each comparison is illustrated separately.

Table 13
S_{11} simulation vs measurement comparisson (blade antena)

Concept	7.5cm	12.5cm	22.5cm	32.5cm	45.5cm
Simulation min. freq. @-10dB (MHz)	100	100	100	100	142
Measurement min. freq. @-10dB (MHz)	112	112	111	111	117
Simulation max. freq. @-10dB (MHz)	141	144	152	164	196
Measurement max. freq. @-10dB (MHz)	145	149	158	166	179
Simulation BW (bandwidth) (MHz)	41	44	52	64	54
Measurement BW (bandwidth) (MHz)	33	37	47	55	62
Simulation min. gain (dB)	-19.58	-21.23	-27.50	-47.14	-26.98
Measurement min. gain (dB)	-15.81	-16.50	-19.72	-41.91	-28.45
Simulation frequency @ min. gain (MHz)	117	118	124	135	163
Measurement frequency @ min. gain (MHz)	126	124	124	126	161

Note. Blade antenna S_{11} simulations and measurements comparison for each balun tuner position.

Regarding the 7.5 cm position, a 9 MHz shift of the S_{11} (@ minimum gain frequency) response is observed between the simulations and the measurements. The simulations present a peak at 117 MHz at 126 MHz (top left), thus obtaining a 9 MHz difference. From this behavior and making a sweep against the other graphs, a shift towards higher frequencies can be seen until they are equalized at 22.5 cm balun position. From this position, the trend changes, and the simulations move forward in frequency: 6 MHz of difference at 12.5 cm (top right), 9 MHz at 32.5 cm (middle left), and 2 MHz at 45.5 cm (middle right). The tuner balun position where the simulations and measurements coincided in frequency (124 MHz) is 22.5 cm (center bottom). With this criterion,

Figure 25

S_{11} simulation vs measurement plots (antena 1:1)

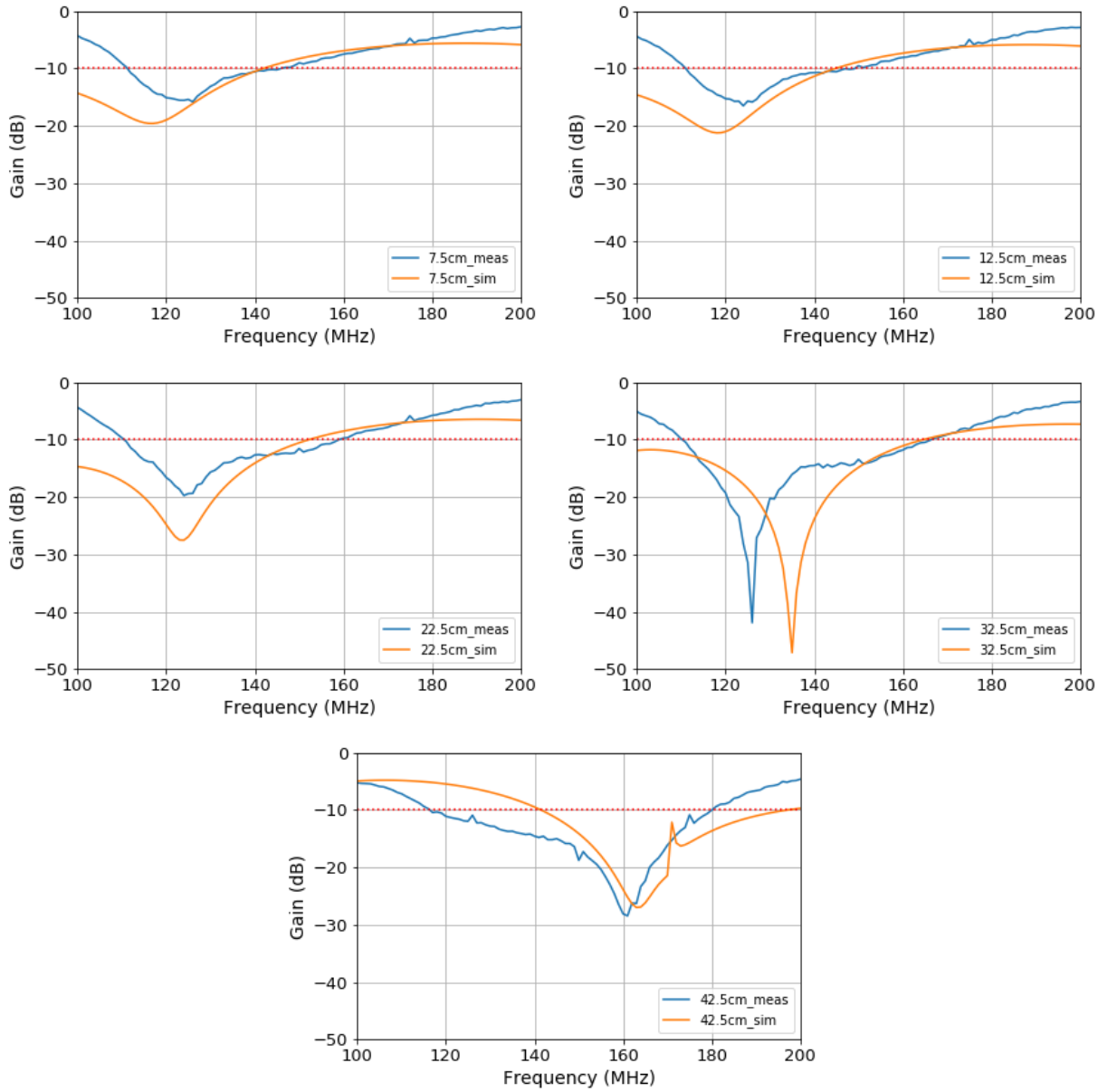

Note. Simulation vs measurement comparison @ 7.5 cm (top left), 12.5 cm (top right), 22.5 cm (middle left), 32.5 cm (middle right) and 42.5 cm (bottom) balun height (position). Ansys HFSS license from Universidad de Chile.

it is recommended that the tuner balun should be at that height from the ground plane.

5.5. SDR measurement comparison

Although all the tested devices are SDR-based, each radio has a distinctive behavior; this is mainly due to different ADCs devices and use of filter banks (for inner SDR filtering stages). Different noise floors are identified for each receiver. Figure 26 illustrates the sensitivity comparison between the three receivers used (Limenet mini, Ettus E310, and USRP 2920). When injecting a fixed signal at 150 MHz, varying the injected gain and setting the receiver at 0 dB (left) and 30 dB (right) gains. The Limenet mini has a noise floor of -78.39 dB, the Ettus E310 -108.46 dB and the USRP 2920 -107.7 dB. The Ettus E310 exhibits the best linearity performance when comparing its response to the spectrum analyzer reference measurement.

When performing the measurements and varying the receiver gains between 0 and 60 dB, the optimum operating point of the 3 SDR devices was at 30 dB. Increasing the gain with values higher than 30 dB resulted in either distortion of the injected signal or generation of parasitic waves (graph). Similar responses were found when configuring different SDRs gains contrasted with the reference model of the spectrum analyzer. For the Lime corresponds to a gain of 30 dB, for the Ettus 20 dB, and for the USRP 0dB.

In terms of the linear response of the SDRs, when injecting a fixed gain of -30 dB and varying the frequency (see Figure 18), the best response was obtained using the USRP2920. It can be seen that the most similar response is achieved with such a device.

The receiver measurements' results define a criterion for the system noise temperature treatment and, hence, the design requirements for the preamplifier. Given the low-intensity levels of the

studied waves and the calculations made regarding the noise temperature of the system (Friss noise temperature model), it is essential to use a double amplification and filtering stage, as a minimum, to reduce the total system temperature of the radio telescope.

Figure 26
SDRs sensitivity comparisson

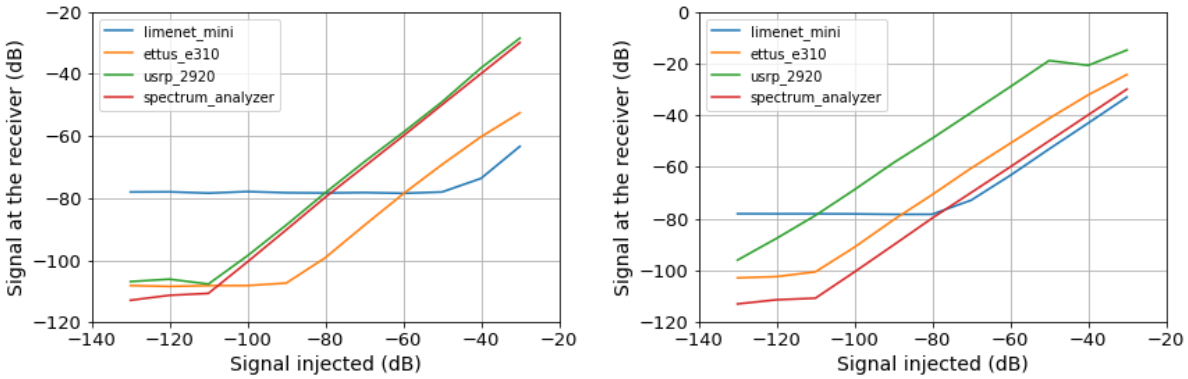

Note. Limenet mini, Ettus E310 and USRP2920 sensitivity comparison @ gain = 0 dB (left) and @ gain = 30 dB (right), injecting 150 MHz and varying the RF level between −30 and −120 dBm.

5.6. Integration of subsystems and data acquisition

The subsystems (antenna, transmission lines, preamplifier, and SDR) were integrated, and the first in-situ measurements were performed (see Figure 27). The implemented preamplifier corresponds to the one suggested in section 5.3.2. The Ettus E310 was used as the receiving SDR system due tothe sensitivity performance, and was configured with a gain of 0 dB. The software used and the FFT configuration correspond to the one referenced in section 2.3.3. Figures 28 and 29 illustrate the measurements performed in the Berlin Paramo.

As mentioned in section 2.3, the display of each frequency range corresponds to 16 MHz windows. The spectra received from 100 to 212 MHz are segmented into seven plots. The pre-

Figure 27
In-situ measurements

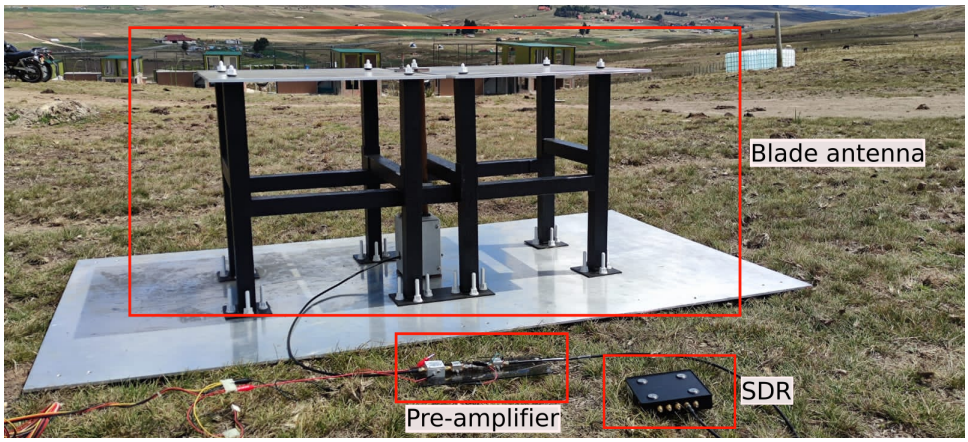

Note. Integrated radiotelescope in Páramo de Berlín.

amplifier's expected behavior was observed considering the previous measurements of the individual elements and the calculations performed. This solution generates an amplification of both target signals and noise. Hence the importance of implementing a preamplifier with at least two filtering stages to reduce the amplification of noise and parasitic signals.

In addition, measurements were made by performing real-time data processing considering three averaging configurations (Figure 30) [5]. The objective was to experiment with this type of technique. Real-time processing is a growing trend in data processing, especially in interferometry. The reason is simple, reduction of data volumes. Although processing information in real-time requires robust computer systems (processors, RAM), it is valuable to experiment with different techniques to define a successful strategy for pre and post-processing of data for future

[5] A Savitsky-Golay digital filter was used, which by means of a convolution process performs the adjustment of points by varying the number of integration polynomials. For low averaging 9 polynomials were used, for medium averaging 6 polynomials and for high averaging 3 polynomials.

Figure 28
In-situ measurements

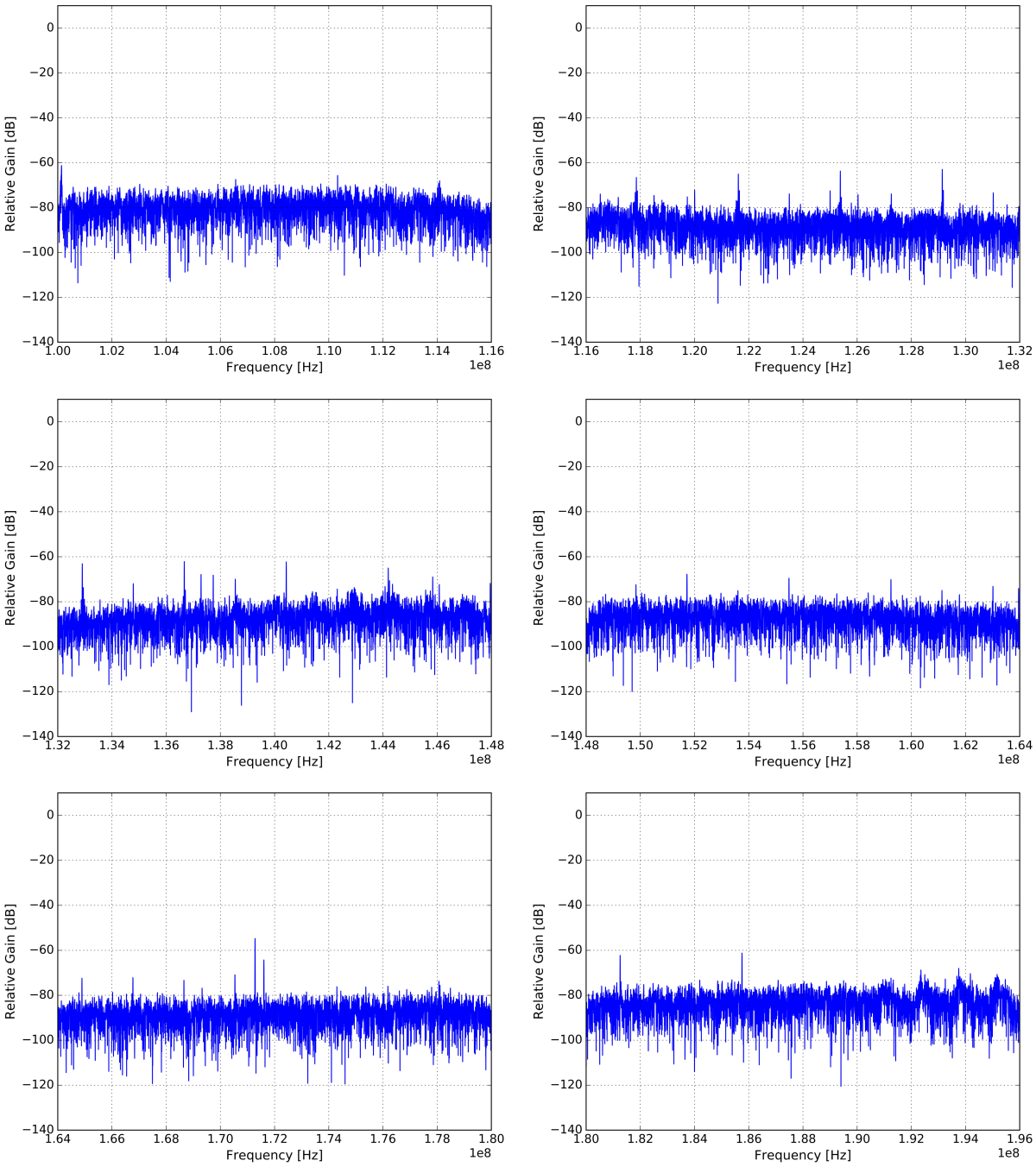

Note. In-situ measurements considering the following frequency ranges: 100-116 MHz (top left), 116-132 MHz (top right), 132-148 MHz (middle left), 148-164 MHz (middle right), 164-180 MHz (bottom left), and 180-196 MHz (bottom right).

Figure 29
In-situ measurements

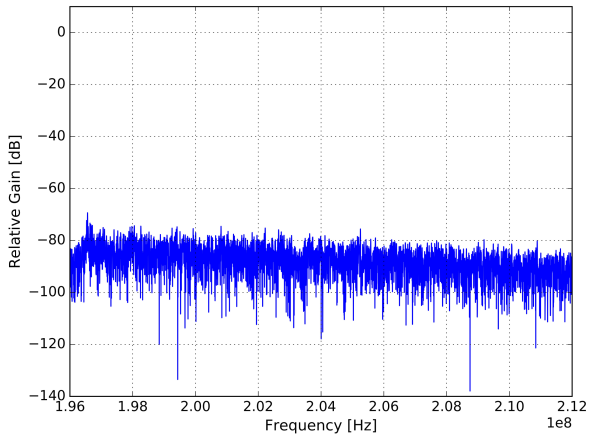

Note. In-situ measurements for a frequency range between 196-212 MHz.

radio telescopes and radio astronomy projects at the UIS.

Data acquisition for a frequency range between 100 and 200 MHz weighs 52.6 MB represented in 6 non-averaged plots and six plots with three averaging levels each and the .txt file where the data is contained. These data are used to guide the definition of hardware and data storage requirements, according to the projection of future radio astronomy projects to be developed mainly from CEMOS and Radiogis.

As complementary results of this project, 6 manuals were developed. These manuals are focused on the use and calibration of a VNA, HFSS dipole simulation guide, and HFSS blade antenna simulation guide. The manuals are in Spanish and English versions. The internal drive of E3T and Radiogis will be used to locate the manuals to be accessible for students and researchers. Also, the folders with the software are located in the same place.

Figure 30

In-situ measurements (with averages)

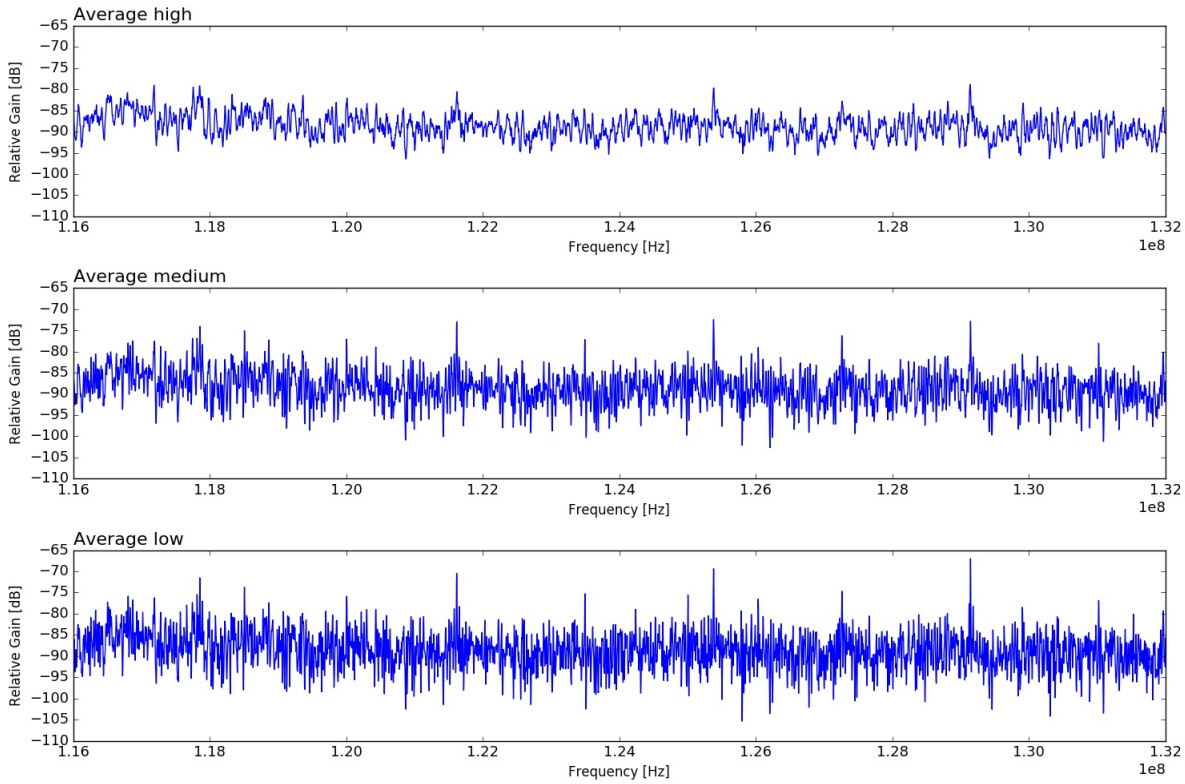

Note. In-situ measurements with high average (top), medium average (middle) and low average (bottom), considering a frequency range between 116 and 132 MHz.

6. Future work

There are some recognized topics to be developed in order to continue with the radio astronomy work at the UIS:

- Establish site survey protocols (ground resistivity, RFI, climatological parameters) using CASIRI instrument from UIS and ProFis instrument from UECCI.

- Participation in two approved research projects:

  Desarrollo de un arreglo interferométrico de Radio Telescopios para establecer una estación de Radio Astronomía de la UIS en el Páramo de Berlín, Santander (Ministerio Nacional de Ciencia y Tecnología)

  Caracterización de emisiones electromagnéticas de interferencia de radiofrecuencias y pruebas de un radiotelescopio (100 MHz) como insumos para la validación del sitio de montaje de una base radio astronómica en la Península Antártica (fase cero dentro del Programa Radio Astronómico Colombiano Antártico (PRAC)) (Comision Colombiana del Oceano).

- Development of 21-cm polynomial adjustement models for data post-processing.

- Development of temperature calibration techniques.

- Collaboration between UIS and Universidad Católica la Santísmima Concepción de Chile to develop radio astronomy initiatives.

- Establish alliances with the international scientific community that studies this specific topic.

7. Conclusions

After carrying out the calculations, simulations, and measurements of the radio telescope, certain conclusions and recommendations were made. On one side, the antenna responded as expected by finding congruence in comparing the simulations to the measurements. This analysis was based on the S11 parameter, gain (linear and normalized), chromaticity and antenna response for planes phi 0 and phi 90. The obtained results, antenna BW = 47 MHz at 124 MHz considering a balun position of 22.5cm, concur theoretically and experimentally. In terms of how the balun modifies the obtained signal, considering S11, it was found that the higher the balun tuner height is, the shift towards higher resonant frequencies also is.

As for the SDRs, a response variation was observed among the measured devices. Initially, it was proposed to validate the Limenet mini exclusively. However, in the process, it was discovered that it was wise to perform the same tests on different SDR devices to achieve such validity. The noise floor levels found (between -80 dB and 110 dB) and the Friss model's system temperature calculations show that a robust pre-amplification stage is required. Testing 3 SDR receivers allowed us to obtain a range of noise floors to consider when sizing the pre-amplification stage. In our case, this situation was confronted by designing a pre-amplification system with two stages of amplification and filtering, reducing the system temperature considerably.

According to related projects such as (Jambagi, 2019), the sensitivity ranges found (between -60 and -110 dB) are permissible for our scientific case. The same case is presented when considering the temperature of the receiving stage (front-end excluding antenna temperature). Ac-

cording to the literature, receiver temperatures were found between 50 (Tingay et al., 2013) and 150 K (Cheng et al., 2018), which agrees with the temperature obtained for the suggested pre-amplifier (143 K). Considering the SDR noise floor and system temperature, it is concluded that further work is required, although the evaluated subsystems respond consistently to the requirements. The next step is to perform calibration of the radio telescope in temperature, accompanied by the post-processing of data using polynomial fitting of 21-cm models and galactic and extra-galactic foreground. It is also recommended to perform measurement campaigns with the 3 SDRs to compare the results of each one.

Building dedicated antennas requires different techniques and types of machinery such as lathe, CNC machining, and diverse welding techniques. Soldering aluminum and copper requires high temperatures to achieve effective soldering traditionally performed for large-scale models or applications. In our case, this has to be performed for scale models, which demands an effective and accurate soldering procedure. The process of building instrumentation for radio astronomy demands high levels of precision. From our experience, this process required the development of unconventional techniques to achieve the proposed objectives. It is exciting and valuable to learn from all the processes immersed when designing, building, and characterizing a radio telescope. Although this project reaches its culmination, it is part of a process to establish a reliable operating system and define the protocols that must be considered when designing, implementing, and validating a radio telescope.

Finally, considering the radio astronomy multidisciplinary teams in universities, research groups, and institutes globally, it is worth recognizing this radio telescope as a catalyst to gener-

ate long-term work at UIS. This work should be structured through the communion of different academic branches and areas of knowledge, in the pursuit of a national-scientific contribution.

Bibliography

Ali, S. (2004). The cosmic microwave background radiation fluctuations from hi perturbations prior to reionization. *Monthly Notices of the Royal Astronomical Society*, 352:142 – 146.

Arnold, S. (2020). *The Software-Defined Radio (SDR)*, pages 221–230.

Barkana, R. and Loeb, A. (2005). Detecting the earliest galaxies through two new sources of 21 centimeter fluctuations. *Astrophysical Journal - ASTROPHYS J*, 626:1–11.

Bowman, J., Rogers, A., Monsalve, R., Mozdzen, T., and Mahesh, N. (2018). An absorption profile centred at 78 megahertz in the sky-averaged spectrum. *Nature*, 555(7694):67–70.

Burke, B. F. and Graham-Smith, F. (2009a). *An Introduction to Radio Astronomy*. Cambridge University Press, 3 edition.

Burke, B. F. and Graham-Smith, F. (2009b). *The origins of radio astronomy*, page 412–420. Cambridge University Press, 3 edition.

Cheng, C., Parsons, A. R., Kolopanis, M., Jacobs, D. C., Liu, A., Kohn, S. A., Aguirre, J. E., Pober, J. C., Ali, Z. S., Bernardi, G., Bradley, R. F., Carilli, C. L., DeBoer, D. R., Dexter, M. R., Dillon, J. S., Klima, P., MacMahon, D. H. E., Moore, D. F., Nunhokee, C. D., Walbrugh, W. P., and Walker, A. (2018). Characterizing signal loss in the 21-cm reionization power spectrum: A revised study of PAPER-64. *The Astrophysical Journal*, 868(1):26.

Costa, André A. Landim, R. C. G. . W. B. . A. E. (2018). Interacting dark energy: possible explanation for 21-cm absorption at cosmic dawn. *The European Physical Journal*, 78(1):26.

DeBoer, D. R., Parsons, A. R., Aguirre, J. E., Alexander, P., Ali, Z. S., Beardsley, A. P., Bernardi, G., Bowman, J. D., Bradley, R. F., Carilli, C. L., Cheng, C., de Lera Acedo, E., Dillon, J. S., Ewall-Wice, A., Fadana, G., Fagnoni, N., Fritz, R., Furlanetto, S. R., Glendenning, B., Greig, B., Grobbelaar, J., Hazelton, B. J., Hewitt, J. N., Hickish, J., Jacobs, D. C., Julius, A., Kariseb, M., Kohn, S. A., Lekalake, T., Liu, A., Loots, A., MacMahon, D., Malan, L., Malgas, C., Maree, M., Martinot, Z., Mathison, N., Matsetela, E., Mesinger, A., Morales, M. F., Neben, A. R., Patra, N., Pieterse, S., Pober, J. C., Razavi-Ghods, N., Ringuette, J., Robnett, J., Rosie, K., Sell, R., Smith, C., Syce, A., Tegmark, M., Thyagarajan, N., Williams, P. K. G., and Zheng, H. (2017). Hydrogen epoch of reionization array (HERA). *Publications of the Astronomical Society of the Pacific*, 129(974):045001.

Ellingson, S., Clarke, T., Cohen, A., Craig, J., Kassim, N., Pihlström, Y., Rickard, L., and Taylor, G. (2009). The long wavelength array. *Proceedings of the IEEE*, 97:1421 – 1430.

Feng, W., Friedt, J., and Wan, P. (2021). Sdr implemented ground-based interferometric radar for displacement measurement. *IEEE Transactions on Instrumentation and Measurement*, pages 1–1.

Furlanetto, S. R., Peng Oh, S., and Briggs, F. H. (2006). Cosmology at low frequencies: The 21cm transition and the high-redshift universe. *Physics Reports*, 433(4-6):181–301.

Jambagi, A. (2019). Design of a Cubesat Based Radio Receiver to Detect the Global EoR Signature. *Arizona State University, Master Thesis*.

Keller, R., Staufenbiel, B., and Aderhold, N. (2015). Software defined radio in radio astronomy; limits and application in rfi detection. In *2015 1st URSI Atlantic Radio Science Conference (URSI AT-RASC)*, pages 1–1.

Mazumder, A. and Datta, A. (2019). Probing the first structures with the ska. In *2019 URSI Asia-Pacific Radio Science Conference (AP-RASC)*, pages 1–2.

Monsalve, R., Rogers, A., Bowman, J., and Mozdzen, T. (2017a). Results from edges high-band: I. constraints on phenomenological models for the global 21 cm signal. *The Astrophysical Journal*, 847.

Monsalve, R. A., Bowman, J. D., Rogers, A. E. E., Mozdzen, T. J., and Mahesh, N. (2018). Extracting the global cosmological 21-cm signal from edges data using mcmc. In *2018 2nd URSI Atlantic Radio Science Meeting (AT-RASC)*, pages 1–1.

Monsalve, R. A., Rogers, A. E. E., Bowman, J. D., and Mozdzen, T. J. (2017b). Calibration of the edges high-band receiver to observe the global 21 cm signature from the epoch of reionization. *The Astrophysical Journal*, 835(1):49.

Mozdzen, T. J., Bowman, J. D., Monsalve, R. A., and Rogers, A. E. E. (2016). Limits on foreground subtraction from chromatic beam effects in global redshifted 21 cm measurements. , 455(4):3890–3900.

Offringa, A. R. and de Bruyn, A. G. (2011). Interference detection results with lofar. In *2011 XXXth URSI General Assembly and Scientific Symposium*, pages 1–4.

Ord, S. M., Tremblay, S. E., McSweeney, S. J., Bhat, N. D. R., Sobey, C., Mitchell, D. A., Hancock, P. J., and Kirsten, F. (2019). Mwa tied-array processing i: Calibration and beamformation. *Publications of the Astronomical Society of Australia*, 36.

Ortega, B. and Reyes, T. (2020). *Comunicaciones Digitales basadas en radio definida por software*. E3T Universidad Industrial de Santander – UIS.

Parsons, A. R. (2011). Exploring the epoch of reionization with low-frequency radio telescopes. In *2011 XXXth URSI General Assembly and Scientific Symposium*, pages 1–2.

Price, D. C., Greenhill, L. J., Fialkov, A., Bernardi, G., Garsden, H., Barsdell, B. R., Kocz, J., Anderson, M. M., Bourke, S. A., Craig, J., Dexter, M. R., Dowell, J., Eastwood, M. W., Eftekhari, T., Ellingson, S. W., Hallinan, G., Hartman, J. M., Kimberk, R., Lazio, T. J. W., Leiker, S., MacMahon, D., Monroe, R., Schinzel, F., Taylor, G. B., Tong, E., Werthimer, D., and Woody, D. P. (2018). Design and characterization of the Large-aperture Experiment to Detect the Dark Age (LEDA) radiometer systems. *Monthly Notices of the Royal Astronomical Society*, 478(3):4193–4213.

Pritchard, J. R. and Loeb, A. (2012). 21 cm cosmology in the 21st century. *Reports on Progress in Physics*, 75(8):086901.

Raghunathan, A., Shankar, N. U., and Subrahmanyan, R. (2013). An Octave Bandwidth Frequency

Independent Dipole Antenna. *IEEE Transactions on Antennas and Propagation*, 61(7):3411–3419.

Ragoomundun, N. and Beeharry, G. (2019). A hybrid sdr-gpu receiver for a low-frequency array in radio astronomy. *Experimental Astronomy*, 47.

Restrepo, O. A., Lucero, F. I., Molina, R., Chaparro, G., Mena, F. P., and R., B. (2020). *Design and analysis of a prototype antenna for the low frequency radio telescope MIST*, pages 65–66.

Roger, A. E. (2012). *EDGES Group Memo 087*. Massachusetts institute of technology Haystack Observatory.

Saptarshi, H. (2018). *Timing delay characterization of GNU Radio based 802.15.4 network using LimeSDR*. University of Stockholm Sweden.

Singh, S., Subrahmanyan, R., Shankar, N. U., Rao, M. S., Girish, B. S., Raghunathan, A., Somashekar, R., and Srivani, K. S. (2018). Saras 2: a spectral radiometer for probing cosmic dawn and the epoch of reionization through detection of the global 21-cm signal. *Experimental Astronomy*, 45(2):269–314.

Sokolowski, M., Tremblay, S. E., Wayth, R. B., Tingay, S. J., Clarke, N., Roberts, P., Waterson, M., Ekers, R. D., Hall, P., Lewis, M., and et al. (2015). Bighorns - broadband instrument for global hydrogen reionisation signal. *Publications of the Astronomical Society of Australia*, 32.

Thyagarajan, N., Parsons, A. R., DeBoer, D. R., Bowman, J. D., Ewall-Wice, A. M., Neben, A. R., and Patra, N. (2016). EFFECTS OF ANTENNA BEAM CHROMATICITY ON REDSHIFTED

21 cm POWER SPECTRUM AND IMPLICATIONS FOR HYDROGEN EPOCH OF REIONIZATION ARRAY. *The Astrophysical Journal*, 825(1):9.

Tingay, S. J., Goeke, R., Bowman, J. D., Emrich, D., Ord, S. M., Mitchell, D. A., Morales, M. F., Booler, T., Crosse, B., Wayth, R. B., Lonsdale, C. J., Tremblay, S., Pallot, D., Colegate, T., Wicenec, A., Kudryavtseva, N., Arcus, W., Barnes, D., Bernardi, G., Briggs, F., Burns, S., Bunton, J. D., Cappallo, R. J., Corey, B. E., Deshpande, A., Desouza, L., Gaensler, B. M., Greenhill, L. J., Hall, P. J., Hazelton, B. J., Herne, D., Hewitt, J. N., Johnston-Hollitt, M., Kaplan, D. L., Kasper, J. C., Kincaid, B. B., Koenig, R., Kratzenberg, E., Lynch, M. J., Mckinley, B., Mcwhirter, S. R., Morgan, E., Oberoi, D., Pathikulangara, J., Prabu, T., Remillard, R. A., Rogers, A. E. E., Roshi, A., Salah, J. E., Sault, R. J., Udaya-Shankar, N., Schlagenhaufer, F., Srivani, K. S., Stevens, J., Subrahmanyan, R., Waterson, M., Webster, R. L., Whitney, A. R., Williams, A., Williams, C. L., and Wyithe, J. S. B. (2013). The Murchison Widefield Array: The Square Kilometre Array Precursor at Low Radio Frequencies. 30:e007.

Vacaliuc, B., Oxley, P., Fields, D., Kurtz, S., and Leech, M. (2012). Rasdr: Benchtop demonstration of sdr for radio astronomy. *Conference: Annual meeting of the Society of Amateur Radio Astronomers, Green Bank, WV, USA, 20120624, 20120627*.

Wilson, T., Rohlfs, K., and Huttemeister, S. (2012). Tools of radio astronomy, 5th edition.

Yuan, X., Dong, L., Wang, M., Guo, S., and Gao, G. (2018). Design and simulation of v-type dipole antenna. In *2018 12th International Symposium on Antennas, Propagation and EM Theory (ISAPE)*, pages 1–4.

Appendix

Appendix A. Scientific production

- A1 Proceeding accepted to be presented in the IEEE International Symposium on Antennas & Propagation & USNC-URSI Radio Science Meeting to be held in Denver Colorado, USA, July 2022.
- A2 Letter of acceptance to attend and present in the 5th Global 21-cm Workshop hosted at the University of Berkeley, October 2022.
- A3 Cover of the accepted project Ministerio Nacional de Ciencia y Tecnología.
- A4 Cover of the accepted project to the VII Expedición Científica de Colombia a la Antártica verano austral 2021-2022.

100-200 MHz sdr-based radio telescope focused on the cosmological study of the Epoch of Reionization

Felipe P. Mosquera[1], Julian Rodriguez-Ferreira[1], Efren Acevedo[1], Oscar Restrepo[2][3], and German Chaparro[4]

[1] Universidad Industrial de Santander, Bucaramanga, Colombia, http//www.uis.edu.co
[2] Universidad de Chile, Santiago de Chile, Chile, http//www.uchile.cl
[3] Universidad ECCI, Bogotá, Colombia, http//www.ecci.edu.co
[4] Universidad de Antioquia, Medellin, Colombia, http//www.udea.edu.co

Abstract—Radio astronomy as an observational technique used in Astronomy allows experimental validation of theoretical models based on the study of electromagnetic cosmic waves. Technically speaking, uses dedicated instrumentation (radio telescopes) to acquire such signals. The study, base on the emission of 21-cm of neutral hydrogen at frequencies between 100 and 200 MHz, permits to cover a scientif c case of open study called Epoch of Reionization (EoR) in which we seek to compare physics models with experimental measurements. This paper presents simulations and measurements of the sub-systems of a 100-200 MHz radiotelescope to establish the feseability to use Software Def ned Radio (SDR) technology devices as receptors for low frequency radio telescopes.

I. Introduction

The study of the 21-cm emission line of neutral hydrogen in the Epoch of Reionization (EoR) of the universe is an open scientif c case directed to the study of the mechanisms of formation of the f rst stars and galaxies generated in the early universe [1], as well as the ionization processes of the primordial gas. 2018 detection of this signal reported by the EDGES project , opened an academic and scientif c debate on the non-correspondence of the current physical models vis-à-vis the reported signal (dissimilar amplitude levels with respect to temperature). We present the design and implementation of a complementary prototype of a low frequency radiotelescope. Our prototype considers an independent antenna designed to operate in the frequency range between 100 and 200 MHz.

The system is based on the design of the High Frequency instrument of the EDGES project and includes a novel receiver based on Software Def ned Radio (SDR) technology.

II. Radio telescope description

Our antenna prototype for EoR science is inspired in the High Band EDGES antenna [2], which is a single polarization dipole-like blade antenna. Our antenna is composed of two rectangular aluminum sections (62.5 cm × 48.1 cm) elevated 52 cm from a rigid aluminum plate with dimensions (1.3 m × 1 m) which is used as a ground plane. The structure of the antenna was built in polystyrene due to its low di-electric coeff cients. A Roberts balun was implemented as an adjustable tuner for impedance matching. This balun allows an adjustment of the electrical length and the transmission line impedance. It consists of two copper tubes attached by a movable aluminum plate which serves both to electrically balance the incoming signal and at the same time calibrate the antenna response in terms of the bandwidth (BW) and central frequency. We tested several SDR receiver models for the signal processing stage and GNU radio will be used for data treatment.

III. Simulations and measurements

A. S11 antenna simulations

Electromagnetic antenna simulations were performed using Ansys HFSS (see Figure 1) [3]. Five tuner balun positions or heights were evaluated: 7.5, 12.5, 22.5, 32.5 and 42.5 cm. These positions represent the height at which the balun is located with respect to the ground plane. When considering the BW response, we found that the best S11 response as a function of tuner balun height is at the 22.5 and 32.5 cm positions. At 22.5 cm a BW of 49 MHz and minimum gain level of (−27.50 dB at 124 MHz was obtained. For the 32.5 cm position a BW of 64 MHz is obtained with a minimum gain level of −47.147dB at 135 MHz.

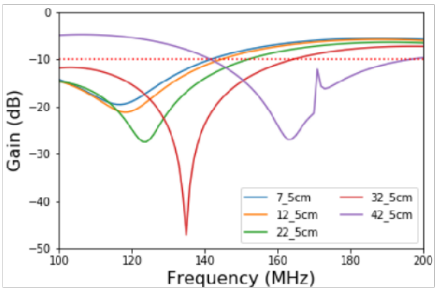

Fig. 1. Comparative S11 vs frequency simulations for the 1:1 antenna considering 5 tuner balun heights.

B. Simulations of antenna chromaticity

Chromaticity in an antenna expresses the level of variation of gain as a function of frequency and direction. Simulations were performed for a 1:1 antenna locating the balun at 22.5 cm. In f rst instance, using HFSS, gain simulations were performed for $\phi = 0^\circ$ and $\phi = 90^\circ$ planes. We processed the simulation data and made the plots using a Python* script [3].

Regarding the variation of gain as a function of frequency for the plane $\phi = 90^\circ$ (see Figure 2), we found a very small

Note. A1 Proceeding accepted to be presented in the IEEE International Symposium on Antennas Propagation.

variation between 118 and 143 MHz. There is a high positive gain variation between 100 and 118 MHz between 0° and 40° and a negative variation between 185 and 200 MHz between 0° and 20°. For elevation higher than 60° the antenna response is optimal since there is no gain variation for all frequencies analyzed.

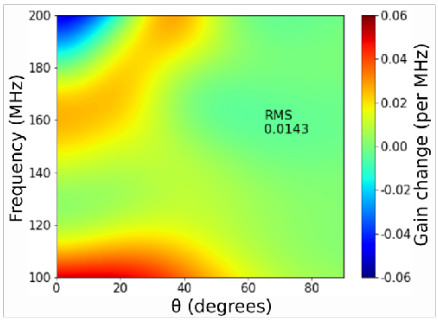

Fig. 2. Antenna chromaticity @ 22.5 cm. for the plane $\phi = 90^{\circ}$.

C. SDR noise measurements

To establish the noise f oor of the SDRs we performed a series of exploratory measurements. Three SDR receivers were tested: Limenet mini, Ettus E310 and USRP 2920 (see Figure 3). A sinusoidal wave with a f xed frequency of 150 MHz was injected to each SDR using a signal generator varying the gain between −30 and −120 dBm. The SDRs were conf gured with gains 0 and 30 dB in order to establish the response under different conf gurations.

Although all the devices were SDR-based, there is a distinctive sensitivity response for each radio; this is mainly due to factors such as different ADCs and f lter banks. Different noise f oors are identif ed for each receiver. The Limenet mini has a noise f oor of −78.39 dB, the Ettus E310 −108.46 dB and the USRP 2920 −107.7 dB.

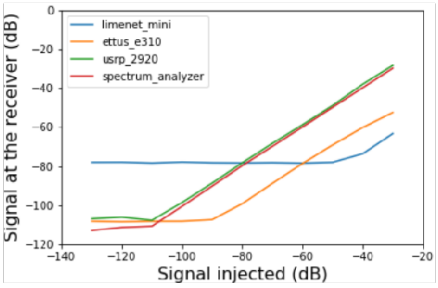

Fig. 3. SDRs sensitivity response @ gain = 0 dB (top), injecting a 150 MHz signal and varying the RF level between −30 and −120 dBm

IV. Results

We intend to use the S11 simulations as reference to benchmark against the real-life performance of the antenna. From these simulations it is possible not only to obtain the BW and center frequency of the antenna, but also to have criteria to def ne the ideal position where the balun tuner should be placed. A frequency shift trend is seen as a function of increasing tuner height. As the height of the balun increases, the frequency response shifts towards higher frequencies. The obtained chromaticity corroborate an optimal theoretical behavior in terms of little-to-no gain variation considering the the expected operational BW of the antenna (between 100 and 149 MHz).

The results of the receiver measurements help def ne the requirements for the system temperature and will therefore constrain the design parameters of the preamplif er. Given the low intensity levels of the expected EoR signals [4] and our calculations of the noise temperature of the system (Friss noise temperature model), we conclude that it is essential to use a double amplif cation and f ltering stage at a minimum. It is then essential to design a custom-design preamplif cation stage considering the additional constraints set by the weakness of the expected EoR signal and the comparatively high galactic background noise.

V. Conclusions

Our simulations and measurements of our proposed prototype antenna and receiver system for EoR signal conf rmation help constrain what the f nal radio telescope design will be. Although SDR technology has been used for radio astronomy applications, the studied scientif c case (EoR) requires additional technical considerations e.g. a robust pre-amplif cation stage. The results obtained serve as a starting point to compare laboratory and in-situ measurements to test the performance of the radio telescope vis-à-vis the simulations shown here, which will help set useful criteria for the validation.

This motivates our current and future work on the following: measuring the electromagnetic performance of a 1:10 scale model of the antenna in an anechoic chamber, S11 antenna measurements of a 1:1 antenna model, and additional testing of the SDRs (gain variation conf gured on the receivers (between −30 dB and −120 dB). With these data it will be possible to establish the feasibility of the radio telescope, considering parameters such as S11, gain, chromaticity, sensitivity and linearity.

ACKNOWLEDGEMENT

*The Python code used to obtain the chromaticity was developed by Restrepo O. and Lucero F., Universidad de Chile and Universidad Católica de la Santísima Concepción.

References

[1] R. Barkana and A. Loeb, "Detecting the earliest galaxies through two new sources of 21 centimeter f uctuations", Astrophysical Journal, vol. 65, 2005, pp. 1–11.

[2] R. Monsalve, A. Rogers, J. Bowman, and T. Mozdzen, "Results from edges high-band: I. constraints on phenomenological models for the global 21 cm signal". The Astrophysical Journal 2017, vol. 847.

[3] O. A. Restrepo, F. I. Lucero, R. Molina, G. Chaparro, F. P. Mena, R. Bustos, "Design and analysis of a prototype antenna for the low frequency radio telescope MIST", Boletín de la Asosiación Argentina de Astronomía, vol. 61c, 2020, pp. 65-66.

[4] S. R. Furlanetto, "Cosmology at Low Frequencies: The 21 Cm Transition and the High-Redshift Universe", Physics Reports, vol. 433, no. 4-6, 2006, pp. 181–301, https://doi.org/info:doi/.

Note. A1 Proceeding accepted to be presented in the IEEE International Symposium on Antennas Propagation.

IEEE International Symposium on Antennas & Propagation
& USNC-URSI Radio Science Meeting
JULY 10-15, 2022 • DENVER 2022apsursi.org

Thursday, 28 April 2022

First Name: [Felipe], Surname: [P. Mosquera]
Universidad Industrial de Santander
Phone: +57 3222240844
Country/Region: Colombia

Dear Felipe P. Mosquera,

Regarding presentation of the following accepted paper:
• 100-200 MHz sdr-based radio telescope focused on the cosmological study of the Epoch of Reionization

We are pleased to inform you that your submission has been accepted for presentation at the 2022 IEEE International Symposium on Antennas and Propagation and USNC-URSI Radio Science Meeting (IEEE AP-S/URSI 2022) in Denver, Colorado, USA, during 10-15 July 2022. Please note that all presentations at the conference will be oral in nature (no poster presentations).

Every accepted paper must be linked to a registered person by 22 May 2022. Any paper not linked to a registered person by this date will be withdrawn from the technical program and proceedings.

All authors should be aware that accepted submissions must be presented at the conference in order to be included in the final proceedings of the conference. Furthermore, as required by IEEE, AP-S/URSI papers will not be submitted to IEEE Xplore if they have not been presented at the conference. A valid presentation at the conference consists of: (1) submitting IEEE copyright forms (for two-page summaries), (2) registering for the conference by the deadline indicated above, and (3) presentation of the paper in person by one of the authors.

At least one author for each submission must register for the conference and pay the required registration fee as described on the conference website, https://2022apsursi.org/. Any author who has not registered will not be able to participate in the conference.

All authors (even those from visa-waiver countries) need to check the current requirements for entering the US. Visa and current travel policies, as well as links to your local embassy or consulate, can be found at the Visa Information web page, https://2022apsursi.org/visa.php. Note that it can take several months for visas to be issued, so we recommend that you start the application process immediately. Questions should be directed to registration@2022apsursi.org.

This letter does not constitute an offer to contribute to the financial costs of registration, travel to or from the conference, or subsistence while in the US. Authors are responsible for the entire travel cost, to and from their home countries, including hotel expenses. Attendees are strongly encouraged to reserve their flights as early as possible in order to optimize their flight schedule.

On behalf of the steering committee, we thank you for submitting this work to the conference. We look forward to welcoming you to AP-S/URSI 2022 in July!

Branislav Notaros
General Chair

Andrew Peterson
Technical Program Chair

Stephen Gedney
TPC Co-Chair

David Jackson
TPC Co-Chair

Karl Warnick
TPC Co-Chair

Billene Cannon
AP-S/URSI 2022 Conference Manager
Conference Management Services, Inc.
2711 Pierre Pl
College Station, Texas, 77845
United States
Phone: +1 979-846-6800
Email: registration@2022apsursi.org

Note. A1 Acceptance letter to present in the IEEE International Symposium on Antennas Propagation.

Berkeley
UNIVERSITY OF CALIFORNIA

Raul A. Monsalve
Assoc. Research Scientist
Space Sciences Laboratory

7 Gauss Way
Berkeley, CA 94720
510 289-3501 phone
raul.monsalve@berkeley.edu
www.raulmonsalve.com

April 05, 2022

To whom it may concern,

This letter is an official invitation to **Felipe Mosquera** to participate in the 5th Global 21-cm Workshop to be hosted at the University of California Berkeley the week of October 17, 2022.

In this scientific workshop we will discuss different aspects of the radio signal expected to have been emitted by neutral hydrogen during the period of formation of the first stars and galaxies in the Universe. At the workshop, **Felipe Mosquera** will give a presentation on recent developments to detect and interpret the expected signal, in addition to participating in discussions and interactions with colleagues. The participation of **Felipe Mosquera** will greatly benefit the scientific outcome of this workshop.

For this workshop there is no registration fee, and the participants are expected to cover all their travel expenses.

Please feel free to contact me in case of any question. My contact information is provided above.

Sincerely,

Raul A. Monsalve, PhD
Associate Research Scientist, UC Berkeley Space Sciences Laboratory

on behalf of the Local Organizing Committee.

https://global21cmworkshop.org/2022-berkeley/
global21cmworkshop2022@gmail.com

Note. A2 Letter of acceptance to attend and present in the 5th Global 21-cm Workshop hosted at the University of Berkeley, October 2022.

Desarrollo de un arreglo interferométrico de Radio Telescopios para establecer una estación de Radio Astronomía de la UIS en el Páramo de Berlín (Santander).

Propuesta de investigación a la convocatoria:
CONVOCATORIA PARA EL FORTALECIMIENTO DE CTEI EN INSTITUCIONES DE EDUCACIÓN SUPERIOR DEL MINISTERIO NACIONAL DE CIENCIA Y TECNOLOGÍA

Investigador Principal:
Julián Gustavo Rodríguez Ferreira[1]

Co-Investigadores:
Profesores UIS
Oscar Mauricio Reyes[2]
Homero Ortega[3]
Ricardo Jaimes Rolon[4,5]

Alianza
Felipe Perilla Mosquera[6]

Afiliaciones:
[1]Grupo de Investigación en Control Electrónica Modelado y Simulación - CEMOS
[2]Grupo de Investigación en Conectividad y Procesamiento de Señales – CPS
[3]Grupo de Investigación RadioGis
[4]Grupo de Investigación En Energía Y Medio Ambiente - GIEMA
[1, 2, 3, 4] Escuela de Ingenierías Eléctrica, Electrónica y de Telecomunicaciones E3T.
[5]Escuela de Ingeniería Mecánica
[6]Fundación para el Desarrollo de la Radio astronomía y Tecnologías Aplicadas – F.D.R.T.A. (Fudarta)

Universidad Industrial de Santander.

Bucaramanga, noviembre de 2020

Note. A3 Cover of the accepted project Ministerio Nacional de Ciencia y Tecnología.

CARACTERIZACIÓN DE EMISIONES ELECTROMAGNÉTICAS DE INTERFERENCIA DE RADIOFRECUENCIAS Y PRUEBAS DE UN RADIOTELESCOPIO (100MHz) COMO INSUMOS PARA LA VALIDACIÓN DEL SITIO DE MONTAJE DE UNA BASE RADIO ASTRONÓMICA EN LA PENÍNSULA ANTÁRTICA (FASE CERO DENTRO DEL PROGRAMA RADIO ASTRONÓMICO COLOMBIANO ANTÁRTICO (PRAC))

Propuesta de investigación a la convocatoria:
VIII CONVOCATORIA ANTÁRTICA EXPEDICIÓN CIENTÍFICA DE COLOMBIA A LA ANTÁRTICA VERANO AUSTRAL 2021– 2022

Investigador Principal:

Julián Gustavo Rodríguez Ferreira[1]

Co-Investigadores:

Felipe Perilla Mosquera[1]
Edison Andrés Soto Ríos[2]
Oscar Mauricio Reyes[3]
Homero Ortega[4]

Afiliaciones:
[1]Grupo de Investigación en Control Electrónica Modelado y Simulación - CEMOS
[2]Grupo de Investigación en Sistemas de Energía Eléctrica - GISEL
[3]Grupo de Investigación en Conectividad y Procesamiento de Señales – CPS
[4]Grupo de Investigación RadioGis
[1, 2, 3, 4] Escuela de Ingenierías Eléctrica, Electrónica y de Telecomunicaciones E3T.

Universidad Industrial de Santander.

Bucaramanga, octubre de 2020

Note. A4 Cover of the accepted project to the VII Expedición Científica de Colombia a la Antártica verano austral 2021-2022

Appendix B. In-situ measurements with averages

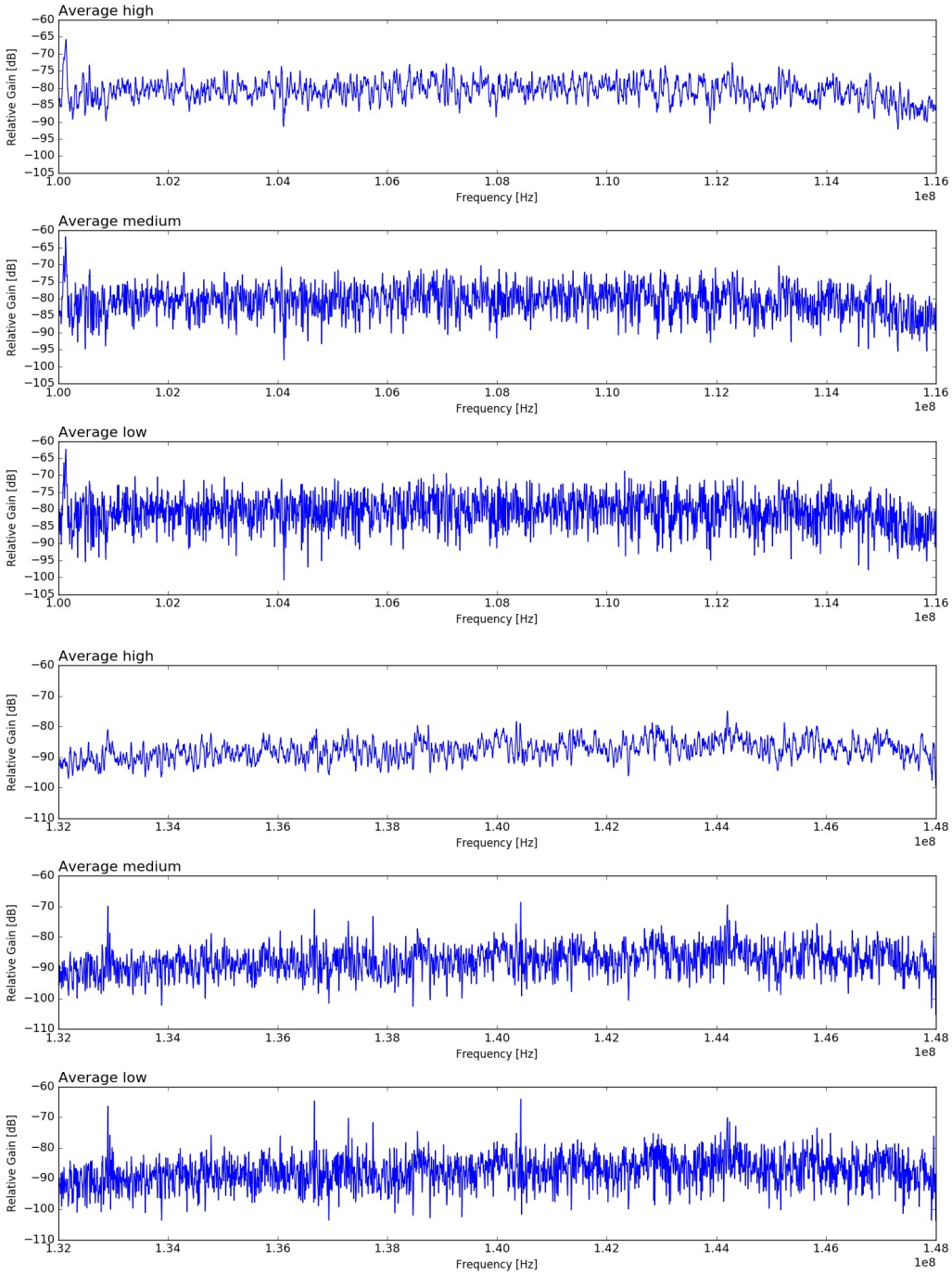

Note. In-situ measurements with high, medium and low average. The first, second, and third plots correspond to a frequency range between 100 and 116 MHz from top to bottom. The fourth, fifth, and sixth plots correspond to a frequency range between 132 and 148 MHz from top to bottom.

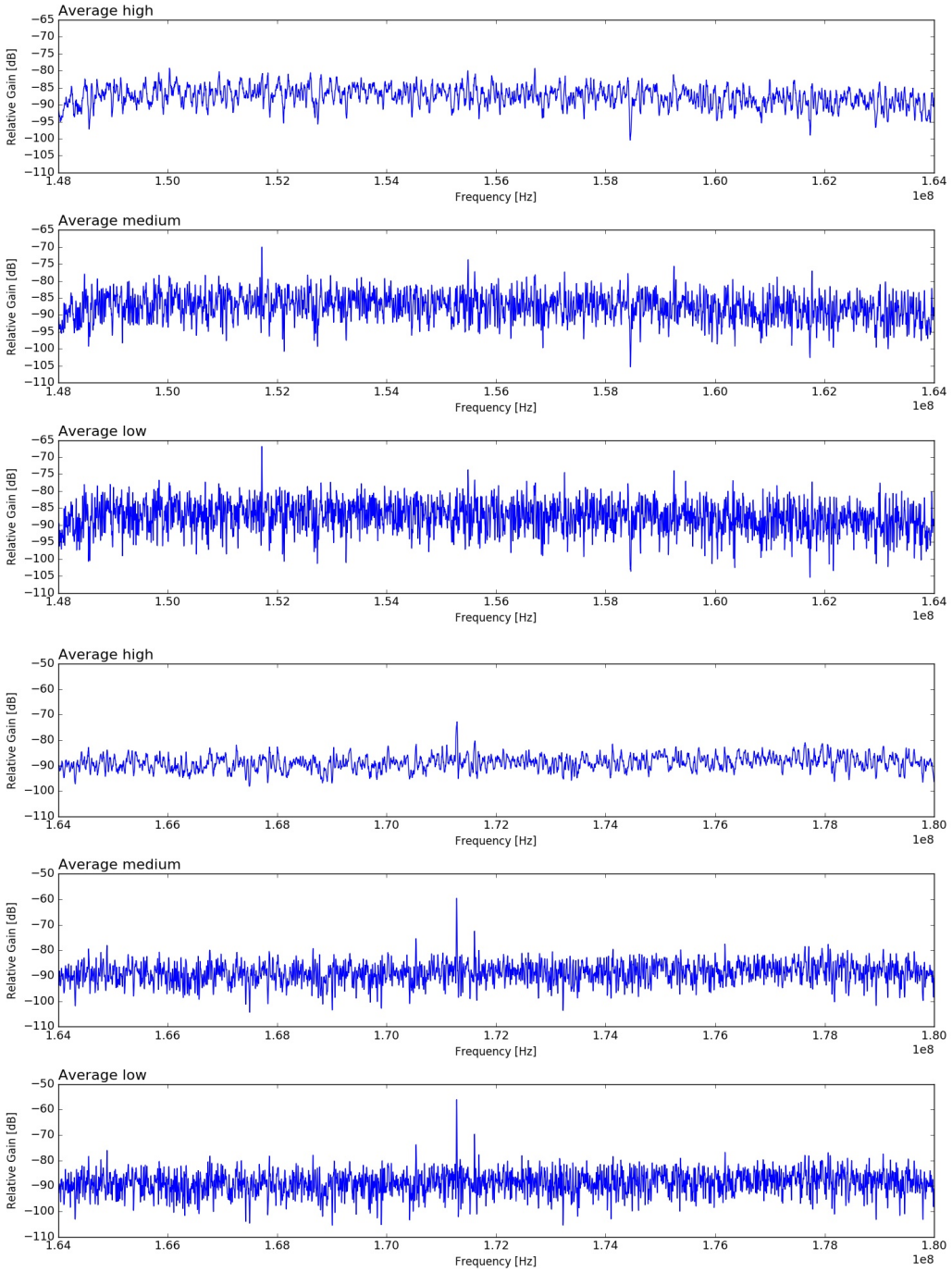

Note. In-situ measurements with high, medium and low average. The first, second, and third plots correspond to a frequency range between 148 and 164 MHz from top to bottom. The fourth, fifth, and sixth plots correspond to a frequency range between 164 and 180 MHz from top to bottom.

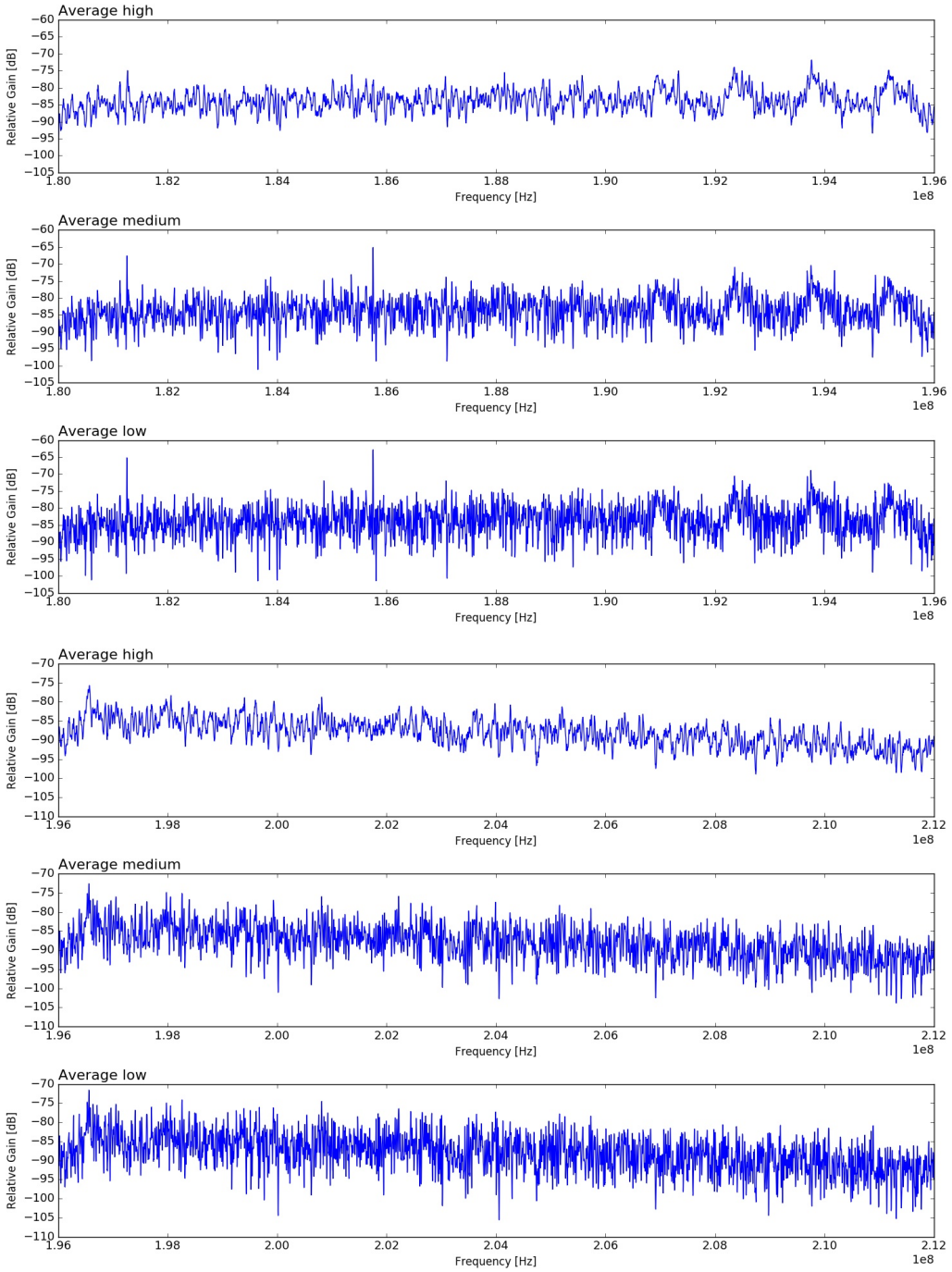

Note. In-situ measurements with high, medium and low average. The first, second, and third plots correspond to a frequency range between 180 and 196 MHz from top to bottom. The fourth, fifth, and sixth plots correspond to a frequency range between 196 and 212 MHz from top to bottom.

Appendix C. Photographs

Note. CNC machining in D'Marco workshop (top left right), late machining in UECCI workshop (center left and right), antenna assembly (bottom left) and component welding in D'Marco workshop (bottom right).

Note. VNA measurements of the 1:10 antenna in UECCI laboratory (top left), SDR measurements in UIS laboratory (top right), VNA measurements of the 1:10 antenna in UIS laboratory (middle) and in-situ measurements with the radiotelescope fully integrated.